

# Uncertainty quantification in metric spaces

Gábor Lugosi<sup>1,2,3</sup> and Marcos Matabuena<sup>\*4,5</sup>

<sup>1</sup>Department of Economics and Business, Pompeu Fabra University, Barcelona, Spain

<sup>2</sup>ICREA, Pg. Lluís Companys 23, 08010 Barcelona, Spain

<sup>3</sup>Barcelona Graduate School of Economics

<sup>4</sup>Department of Biostatistics, Harvard University, Boston, MA 02115, USA

<sup>5</sup>Universidad de Santiago de Compostela

May 9, 2024

## Abstract

This paper introduces a novel uncertainty quantification framework for regression models where the response takes values in a separable metric space, and the predictors are in a Euclidean space. The proposed algorithms can efficiently handle large datasets and are agnostic to the predictive base model used. Furthermore, the algorithms possess asymptotic consistency guarantees and, in some special homoscedastic cases, we provide non-asymptotic guarantees. To illustrate the effectiveness of the proposed uncertainty quantification framework, we use a linear regression model for metric responses (known as the global Fréchet model) in various clinical applications related to precision and digital medicine. The different clinical outcomes analyzed are represented as complex statistical objects, including multivariate Euclidean data, Laplacian graphs, and probability distributions.

**Keywords:** Uncertainty Quantification; Metric Spaces; Conformal Prediction; Fréchet Mean; Precision medicine applications.

## 1 Introduction

### 1.1 Motivation and goal

The increasing use of statistical and machine learning algorithms as predictive tools is transforming [Banerji et al., 2023, Hammouri et al., 2023, Matabuena, 2022], and digital markets. Hence, it has become more critical than ever to conduct an uncertainty analysis to create trustworthy predictive models and validate their usefulness [Romano et al., 2019]. Data analysts tend to focus on pointwise estimation through the conditional mean between a response and a set of predictors, neglecting other crucial aspects of the conditional distribution between the involved random variables [Kneib et al., 2021]. In order to quantify the uncertainty of the point estimates, we need to estimate other characteristics of the conditional distribution beyond the conditional mean.

An innovative approach to tackle uncertainty quantification problems involves employing the conformal inference framework, first introduced by Gammerman, Vovk, and Vapnik in 1998 [Gammerman et al., 1998]. Building upon this foundation, Vovk, Gammerman, and Shafer have made significant contributions to the

---

\*mmatabuena@hsph.harvard.edu

field [Vovk et al., 2005]. Conformal inference allows one to construct prediction sets with non-asymptotic guarantees, setting it apart from other methods that only offer asymptotic guarantees.

However, despite its attractive properties and advantages, conformal inference does have some limitations in different settings that include:

1. **Computational Complexity:** The implementation of conformal inference methods can be computationally expensive, especially if data-splitting strategies to estimate the underlying regression model and prediction region (referred to as *conformal-split* in the literature) are not considered [Vovk et al., 2018, Solari and Djordjilović, 2022].
2. **Conservative Intervals:** The method tends to produce conservative intervals if the regression function used is not well-calibrated with respect to the underlying model, or if the conformal inference method is mis-specified [Lu, 2023] (e.g., using a homoscedastic model when the underlying conditional distribution function between the random response variable  $Y$  and the random predictor  $X$  is governed by heteroscedastic random errors).
3. **Limited Applicability:** Conformal inference may have limited applicability, particularly in scenarios with multivariate responses or when the observed data is extracted from complex survey designs where the exchangeability hypothesis can be violated (see [Barber et al., 2023], who quantify the impact of this fact in terms of the total variation distance between distributions).
4. **Asymptotic Guarantees:** In some special cases, other methods may provide stronger asymptotic guarantees compared to the algorithms derived for the conformal inference framework (see [Györfi and Walk, 2019] for a discussion).

In the context of precision and digital medicine, clinical outcomes can take on complex statistical forms such as probability distributions or graphs [Matabuena, 2022], and there is no general methodology available to perform uncertainty analysis in such settings. For instance, in the case of a glucose time series, a modern approach to summarizing the glucose profiles involves using a distributional representation of the time series, such as their quantile functions. As prior research has shown, these new representations [Ghosal and Matabuena, 2023] can capture information about glucose homeostasis metabolism that traditional diabetes biomarkers cannot measure [Matabuena et al., 2021a, Matabuena et al., 2022a, Ghosal et al., 2021a].

This paper proposes a general method to quantify uncertainty in regression modeling for responses taking values in separable metric spaces [Fréchet, 1948, Petersen and Müller, 2019, Schötz, 2021] and Euclidean predictors. The new algorithms can handle large datasets efficiently, work independently of the predictive base model fitted, and offer asymptotic consistency guarantees. We demonstrate the usefulness and applicability of the novel uncertainty quantification framework in practice through several examples in digital and precision medicine.

Below, we introduce the notation and mathematical concepts to define the new uncertainty quantification framework.

## 1.2 Notation and problem definition

Let  $(X, Y) \in \mathcal{X} \times \mathcal{Y}$  be a pair of random variables that play the role of the predictor and response variable in a regression model. We assume that  $\mathcal{X} = \mathbb{R}^p$  and  $\mathcal{Y}$  is a separable metric space equipped with a distance  $d_1$ . We assume that there exists  $y \in \mathcal{Y}$  such that  $\mathbb{E}(d_1^2(Y, y)) < \infty$ . The regression function  $m$  is defined as

$$m(x) = \operatorname{argmin}_{y \in \mathcal{Y}} \mathbb{E}(d_1^2(Y, y) | X = x), \quad (1)$$

where  $x \in \mathbb{R}^p$ . In other words,  $m$  is the conditional Fréchet mean [Petersen and Müller, 2019]. For simplicity, we assume that the minimum in (1) is achieved for each  $x$  and moreover, the conditional Fréchet mean of  $Y$  given  $X = x$ , is unique. We note here that one may also consider the conditional Fréchet median obtained by  $\operatorname{argmin}_{y \in \mathcal{Y}} \mathbb{E}(d_1(Y, y) | X = x)$ . However, this is a special case of our setup obtained by replacing the metric  $d_1$ , by  $\sqrt{d_1}$  (which is also a metric).

Suppose that  $\mathcal{Y}$  is also equipped with another distance  $d_2$ . We may have  $d_2 = d_1$ , but in some cases it is convenient to work with two distances.

For  $y \in \mathcal{Y}$  and  $r \geq 0$ , denote by  $\mathcal{B}(y, r) := \{z \in \mathcal{Y}; d_2(y, z) \leq r\}$ , the closed ball of center  $y \in \mathcal{Y}$ , and radius  $r$ .

**Definition 1.** We say that the distribution of  $(X, Y)$  is homoscedastic with respect to the regression function  $m$  if there exists a function  $\phi : [0, \infty) \rightarrow [0, 1]$  such that for all  $x \in \mathbb{R}^p$  and  $r \geq 0$ ,

$$\mathbb{P}(Y \in \mathcal{B}(m(x), r) | X = x) = \phi(r).$$

To motivate better our definition of homoscedasticity, let us consider the following examples. The first example is the most natural and commonly encountered in the statistical literature. In this case, the notion of homoscedasticity aligns with the traditional definition.

However, the second example is non-trivial and serves to illustrate that even in a spaces without a vector-space structure, it is still possible to have statistical models that fall under the homoscedastic regime according to our definition.

**Example 1.** Suppose that  $\mathcal{X} = \mathbb{R}^p$ ,  $\mathcal{Y} = \mathbb{R}^m$ ,  $d_1(\cdot, \cdot) = d_2(\cdot, \cdot) = \|\cdot - \cdot\|$  (arbitrary norm in  $\mathbb{R}^m$ ), and consider the regression model

$$Y = m(X) + \varepsilon, \tag{2}$$

where, the random vector  $\varepsilon$ , taking values in  $\mathbb{R}^m$ , is independent of  $X$ .

Obviously,  $\mathbb{P}(d_2(Y, m(x)) \leq r | X = x) = \mathbb{P}(\|\varepsilon\| \leq r | X = x) = \phi(r)$ , due to the independence of  $\varepsilon$  and  $X$ .

**Example 2.** Consider  $\mathcal{X} = \mathbb{R}^p$  and  $\mathcal{Y} = \mathcal{W}_2(\mathbb{R})$ , where  $\mathcal{W}_2(\mathbb{R})$  denotes the 2-Wasserstein space (see [Major, 1978, Panaretos and Zemel, 2020]). More specifically, we define  $\mathcal{W}_2(\mathbb{R}) = \{F \in \Pi(\mathbb{R})\}$ , where  $\Pi(\mathbb{R})$  is the set of distribution functions over  $\mathbb{R}$  with a finite number of discontinuities.

A natural metric for  $\mathcal{W}_2(\mathbb{R})$  is  $d_{\mathcal{W}_2}^2(F, G)$ , is defined as

$$d_{\mathcal{W}_2}^2(F, G) = \int_0^1 (Q_F(t) - Q_G(t))^2 dt. \tag{3}$$

Here,  $Q_F$  and  $Q_G$  denote the quantile functions of the distribution functions  $F$  and  $G$ , respectively.

Define the discrete-time stochastic process  $Z(\cdot)$  as

$$Z(j) = g(X) + \varepsilon(j), \quad j = 1, \dots, n,$$

where  $X$  is a random vector taking values in  $\mathbb{R}^p$ ,  $g : \mathbb{R}^p \rightarrow \mathbb{R}$  is a continuous function, and for each  $t = 1, \dots, n$ ,  $\varepsilon(t) \sim \mathcal{N}(0, \sigma_\varepsilon^2)$ , with  $\varepsilon(j) \perp \varepsilon(j')$  for  $j \neq j'$ , where  $\perp$  denotes the statistical independence between two random variables, and  $\varepsilon(1), \dots, \varepsilon(n)$  are independent of  $X$ .

Then, we define the element  $F_n \in \mathcal{W}_2(\mathbb{R})$  as

$$F_n(t) = \frac{1}{n} \sum_{j=1}^n \mathbb{I}\{Z(j) \leq t\}. \tag{4}$$

Similarly, we can define the  $\rho$ -th quantile related to  $F_n$  as  $Q_n(\rho) = \inf\{t : F_n(t) \geq \rho\}$ , which has an explicit expression as  $Q_n(\rho) = g(X) + \sum_{j:|j/n| \leq \rho} \varepsilon_{(j)}$ , where  $\varepsilon_{(j)}$  is the  $j$ -th ordered random error value from  $\{\varepsilon(j)\}_{j=1}^n$ . The expectation of the quantile function can be easily derived as:

$$\mathbb{E}(Q_n(\rho) | X) = g(X) + \sigma_\varepsilon h_n(\rho), \quad (5)$$

where  $h_n(\cdot)$  is a function that depends on the sample size  $n$ . To simplify the notation, we denote  $Q_n = [F_n]^{-1}$ . By the definition of the metric  $d_{\mathcal{W}_2}^2(\cdot, \cdot)$ ,  $[m(X)]^{-1}(\rho) = \mathbb{E}[Q_n(\rho)|X]$ . To see this, we note that

$$m(x) = \operatorname{argmin}_{y \in \mathcal{Y}_2(\mathbb{R})} \mathbb{E}(d_{\mathcal{W}_2}^2(F_n, y) | X = x) = \operatorname{argmin}_{y \in \mathcal{Y}_2(\mathbb{R})} \mathbb{E} \left( \int_0^1 (Q_n(t) - y^{-1}(t))^2 dt | X = x \right) = \mathbb{E}[Q_n | X = x]^{-1}, \quad (6)$$

where, in the final step, we leverage the property that the mean operator minimizes the aforementioned optimization problem in any Euclidean space.

Then, the squared Wasserstein distance between the distribution function  $F_n$  with respect to its conditional Fréchet mean  $m(X)$  is calculated as:

$$d_{\mathcal{W}_2}^2(F_n, m(X)) = \int_0^1 \left( g(X) + \sum_{j:|j/n| \leq \rho} \varepsilon_{(j)} - g(X) - \sigma_\varepsilon h_n(\rho) \right)^2 d\rho,$$

which does not depend on the value of  $X$ .

We say that the distribution of  $(X, Y)$  is heterocedastic with respect to the regression function  $m$  when

$$\mathbb{P}(Y \in \mathcal{B}(m(x), r) | X = x)$$

may depend on  $x$ .

Given a random observation  $X$ , and confidence level  $\alpha \in [0, 1]$ , our goal is to estimate a prediction region  $C^\alpha(X) \subset \mathcal{Y}$  of the response variable  $Y$  that contains the response variable with probability at least  $1 - \alpha$ . We introduce the population version of the prediction region.

**Definition 2.** We define the oracle-prediction region as

$$C^\alpha(x) := \mathcal{B}(m(x), r(x)), \quad (7)$$

where  $r(x)$  is the smallest number  $r$  such that  $\mathbb{P}(Y \in \mathcal{B}(m(x), r) | X = x) \geq 1 - \alpha$ .

In order to estimate  $C^\alpha(x)$ , suppose that we observe a random sample  $\mathcal{D}_n = \{(X_i, Y_i) \in \mathcal{X} \times \mathcal{Y} : i \in [n] := \{1, 2, \dots, n\}\}$  containing independent, identically distributed (i.i.d.) pairs drawn from the same distribution as  $(X, Y)$ . In the rest of this paper, we split  $\mathcal{D}_n$  in two disjoint subsets,  $\mathcal{D}_n = \mathcal{D}_{\text{train}} \cup \mathcal{D}_{\text{test}}$ , in order to estimate the center and radius of the ball with two independent random samples. We denote the set of indexes  $[S_1] := \{i \in [n] : (X_i, Y_i) \in \mathcal{D}_{\text{train}}\}$ ,  $[S_2] := \{i \in [n] : (X_i, Y_i) \in \mathcal{D}_{\text{test}}\}$ , and we denote  $|\mathcal{D}_{\text{train}}| = n_1$  and  $|\mathcal{D}_{\text{test}}| = n_2 = n - n_1$ .

We propose estimators of the oracle-prediction region  $C^\alpha(x)$  of the form  $\tilde{C}^\alpha(x) = \mathcal{B}(\tilde{m}(x), \tilde{r}_\alpha(x))$ , where  $\tilde{m}(x)$  and  $\tilde{r}_\alpha(x)$  are estimators of  $m(x)$  and  $r_\alpha(x)$ . For simplicity, we assume that the outcomes of the estimator  $\tilde{m}(\cdot; \mathcal{D}_{\text{train}})$  remain unaffected by the order in which the random elements of  $\mathcal{D}_{\text{train}}$  are considered during the estimation process (i.e., the estimator is permutation-invariant). This technical requirement is commonly introduced in the context of conformal inference algorithms.

**Definition 3.** Consider a measurable mapping  $C : \mathcal{X} \rightarrow 2^{\mathcal{Y}}$ . We define the error of  $C$  with respect to the oracle-prediction region as

$$\varepsilon(C, x) = \mathbb{P}(Y \in C(X) \Delta C^\alpha(X) \mid X = x),$$

where  $\Delta$  denotes the symmetric difference.

If  $C = \tilde{C}$ , is constructed from  $\mathcal{D}_n$ , then

$$\varepsilon(\tilde{C}, x) = \mathbb{P}(Y \in \tilde{C}(X) \Delta C^\alpha(X) \mid X = x, \mathcal{D}_n).$$

We are interested in the integrated error

$$\mathbb{E}(\varepsilon(\tilde{C}, X) \mid \mathcal{D}_n).$$

We say that  $\tilde{C}$  is consistent if

$$\lim_{n \rightarrow \infty} \mathbb{E}(\varepsilon(\tilde{C}, X) \mid \mathcal{D}_n) \rightarrow 0 \text{ in probability.} \quad (8)$$

### 1.3 Contributions

Now, we summarize the main contributions of this paper:

1. We propose two uncertainty quantification algorithms, one for the homoscedastic case and another one for the general case.
  - (a) Homoscedastic case: We propose a natural generalization of split conformal inference techniques [Vovk et al., 2018, Solari and Djordjilović, 2022] in the context of metric space responses. We obtain non-asymptotic guarantees of marginal coverage of the type  $\mathbb{P}(Y \in \tilde{C}^\alpha(X)) \geq 1 - \alpha$ . In this setting, we also show that  $\tilde{C}$  is consistent, under mild assumptions, which only require the consistency of the conditional Fréchet mean estimator, i.e.,  $\mathbb{E}(d_2(\tilde{m}(X), m(X)) \mid \mathcal{D}_{train}) \rightarrow 0$  in probability as  $|\mathcal{D}_{train}| \rightarrow \infty$ .
  - (b) Heteroscedastic case: We present a novel local algorithm based on the concept of  $k$ -nearest neighbors, initially proposed by Fix and Hodges [Fix and Hodges, 1951] and later extended by Cover [Cover, 1968] (for a contemporary reference on the topic, see [Biau and Devroye, 2015]). While we do not provide non-asymptotic guarantees regarding the marginal coverage of the prediction region, we prove its consistency.
  - (c) The predictions regions are the generalization of the concept of conditioned quantiles for metric space responses. The prediction regions are defined by a center function  $m$  and a specific radius  $r$  corresponding to a chosen probability level,  $\alpha \in [0, 1]$ . This extension builds upon recent advances in the theory of unconditional quantiles for metric spaces [Liu et al., 2022] and provides a natural generalization of the existing concepts.

Importantly, from a computational perspective, after estimating the regression function  $m$ , the uncertainty quantification algorithms are capable of handling problems involving millions of data points in just a few seconds.

2. We introduce an approach to discern between homoscedastic and heteroscedastic uncertainty quantification models using a global hypothesis testing criterion. Unlike classical approaches [Goldfeld and Quandt, 1965], our methods take a general and non-parametric perspective, allowing for wider applicability. We draw upon the concept distance correlation, based on the energy distance initially introduced [Székely et al., 2007a, Székely and Rizzo, 2017]. Our criterion provides a powerful tool to assess the homoscedasticity or heteroscedasticity of the underlying distribution.

3. The proposed uncertainty quantification framework has the potential to develop new models for complex statistical objects for different modeling tasks. In this paper, we focus on a *local* [Boehm Vock et al., 2015] and *general* variable selection method designed specifically for responses in an arbitrary separable metric space. Other existing variable selection methods are limited to linear models and adopt a global perspective [Tucker et al., 2021].
4. We illustrate the potential of the proposed framework in real-world scenarios and demonstrate its performance in applications in the domain of digital and precision medicine [Tu et al., 2020]. The different applications involve probability distributions with the 2-Wasserstein metric, fMRI data with Laplacian graphs, and multivariate Euclidean data. As application of our framework, we discuss an application that provides normative reference values [Wang et al., 2018] for glucose time series in healthy individuals using the recently proposed distributional glucose time series representations [Matabuena et al., 2021a]. This new analysis has the potential to establish clearer characterizations as the glucose values evolve in the healthy population conditioned on patient characteristics, providing a formal basis for establishing personalized definition of diseases. For example, the derivation of reference values across healthy populations has gained increasing interest among digital medical researchers, as demonstrated by the study [Shapiro et al., 2023]. In their research, they defined normative values for a digital biomarker, namely, the "Pulse Oximetry value."

## 1.4 Literature overview

### 1.4.1 Uncertainty quantification

In recent years, uncertainty quantification became an active research area [Geisser, 2017, Politis, 2015]. The impact of uncertainty quantification on data-driven systems has led to a remarkable surge of interest in both applied and theoretical domains. These works delve into the profound implications of uncertainty quantification in statistical science and beyond such as in the biomedical field [Hammouri et al., 2023, Banerji et al., 2023].

Geisser's pioneering book develops a mathematical theory of prediction inference [Geisser, 2017]. Building upon Geisser's foundations, Politis presented a comprehensive methodology that effectively harnesses resampling techniques [Politis, 2015]. Additionally, the book of Vovk, Gammmerman, and Shafer [Vovk et al., 2005] (see recent reviews [Angelopoulos and Bates, 2023, Fontana et al., 2023] here) has been influential.

One of the most widely used and robust frameworks for quantifying uncertainty in statistical and machine learning models is conformal inference [Shafer and Vovk, 2008]. The central idea of conformal inference is rooted in the concept of exchangeability [Kuchibhotla, 2020]. For simplicity, we assume that the random elements observed,  $\mathcal{D}_n$ , are independent and identically distributed (i.i.d.). Now, we present a general overview of conformal inference methods for regression models with scalar responses. Consider the sequence  $\mathcal{D}_n = \{(X_i, Y_i)\}_{i=1}^n$  of i.i.d. random variables. Given a new i.i.d. random pair  $(X, Y)$  with respect to  $\mathcal{D}_n$ , conformal prediction, as introduced by [Vovk et al., 2005], provides a family of algorithms for constructing prediction intervals independently of the regression algorithm used.

Fix any regression algorithm

$$\mathcal{A} : \cup_{n \geq 0} (\mathcal{X} \times \mathbb{R})^n \rightarrow \{\text{measurable functions } \tilde{m} : \mathcal{X} \rightarrow \mathbb{R}\},$$

which maps a data set containing any number of pairs  $(X_i, Y_i)$ , to a fitted regression function  $\tilde{m}$ . The algorithm  $\mathcal{A}$  is required to treat data points symmetrically, i.e.,

$$\mathcal{A}((x_{\pi(1)}, y_{\pi(1)}), \dots, (x_{\pi(n)}, y_{\pi(n)})) = \mathcal{A}((x_1, y_1), \dots, (x_n, y_n)) \quad (9)$$

for all  $n \geq 1$ , all permutations  $\pi$  on  $[n] = \{1, \dots, n\}$ , and all  $\{(x_i, y_i)\}_{i=1}^n$ . Next, for each  $y \in \mathbb{R}$ , let

$$\tilde{m}^y = \mathcal{A}((X_1, Y_1), \dots, (X_n, Y_n), (X, y))$$

denote the trained model, fitted to the training data together with a hypothesized test point  $(X, y)$ , and let

$$R_i^y = \begin{cases} |Y_i - \tilde{m}^y(X_i)|, & i = 1, \dots, n, \\ |y - \tilde{m}^y(X)|, & i = n+1. \end{cases} \quad (10)$$

The prediction interval for  $X$  is then defined as

$$\tilde{C}^\alpha(X; \mathcal{D}_n) = \left\{ y \in \mathbb{R} : R_{n+1}^y \leq Q_{1-\alpha} \left( \sum_{i=1}^{n+1} \frac{1}{n+1} \cdot \delta_{R_i^y} \right) \right\}, \quad (11)$$

where  $Q_{1-\alpha} \left( \sum_{i=1}^{n+1} \frac{1}{n+1} \cdot \delta_{R_i^y} \right)$  denotes the quantile of order  $1 - \alpha$  of the empirical distribution  $\sum_{i=1}^{n+1} \frac{1}{n+1} \cdot \delta_{R_i^y}$ .

The full conformal method is known to guarantee distribution-free predictive coverage at the target level  $1 - \alpha$ :

**Theorem 1** (Full conformal prediction [Vovk et al., 2005]). *If the data points  $(X_1, Y_1), \dots, (X_n, Y_n), (X, Y)$  are i.i.d. (or more generally, exchangeable), and the algorithm  $\mathcal{A}$  treats the input data points symmetrically as in (9), then the full conformal prediction set defined in (11) satisfies*

$$\mathbb{P}(Y \in \tilde{C}^\alpha(X; \mathcal{D}_n)) \geq 1 - \alpha.$$

The same result holds for split conformal methods, which involve estimating the regression function on  $\mathcal{D}_{\text{train}}$  and the quantile on  $\mathcal{D}_{\text{test}}$ .

Conformal inference (both split and full) was initially proposed in terms of “nonconformity scores”  $\hat{S}(X_i, Y_i)$ , where  $\hat{S}$  is a fitted function that measure the extent to which a data point  $(X_i, Y_i)$  is unusual relative to a training data set  $\mathcal{D}_{\text{train}}$ . For simplicity, so far we have only presented the most commonly used nonconformity score, which is the residual from the fitted model

$$\hat{S}(X_i, Y_i) := |Y_i - \tilde{m}(X_i)|, \quad (12)$$

where  $\tilde{m}$  is estimator of the regression function, estimated using random elements from the first split,  $\mathcal{D}_{\text{train}}$ .

The non-asymptotic guarantees provided by Theorem 1 can be achieved under more general conditions. For instance, Vovk [Vovk, 2012] established non-asymptotic guarantees with respect to the conditional coverage probability  $\mathcal{D}_n$ , employing the same hypotheses used in Theorem 1. He proves inequalities of the form

$$\mathbb{P}(Y \in \tilde{C}^\alpha(X; \mathcal{D}_n) \mid \mathcal{D}_n) \geq 1 - \alpha, \quad (13)$$

while Barber et al. [Foygel Barber et al., 2021] investigated the case of conditional coverage probability with respect to a specific point  $x \in \mathcal{X}$ , meaning

$$\mathbb{P}(Y \in \tilde{C}^\alpha(X; \mathcal{D}_n) \mid X = x) \geq 1 - \alpha. \quad (14)$$

However, only in some special cases, such as those involving a finite predictor space, is it possible to generalize the results of Theorem 1.

In the general i.i.d. context, and beyond the conformal inference framework, within the asymptotic regime, Györfi and Walk [Györfi and Walk, 2019] presented a kNN-based uncertainty quantification algorithm

conditioned on both: i) a random sample  $\mathcal{D}_n$ , and ii) covariate characteristics. This algorithm possesses the property that

$$\lim_{n \rightarrow \infty} \mathbb{P}(Y \in \tilde{C}^\alpha(X; \mathcal{D}_n) | \mathcal{D}_n, X = x) = 1 - \alpha \text{ in probability.}$$

The work of [Györfi and Walk, 2019] is particularly relevant as it provides optimal non-parametric rates for kNN-based uncertainty quantification.

Several authors established non-asymptotic guarantees for the coverage outlined in equation (14). However, in general, this is impossible without incorporating strong assumptions about the joint distribution of  $(X, Y)$  or possessing exact knowledge of the distribution [Foygel Barber et al., 2021, Gibbs et al., 2023]. [Lei and Wasserman, 2014] introduced conditions under which the condition in (14) can lead to the Lebesgue measure of the estimated prediction region  $\tilde{C}^\alpha(X; \mathcal{D}_n)$  becoming unbounded under general hypotheses. More specifically, they prove that,

$$\lim_{n \rightarrow \infty} \mathbb{E}[\text{Leb}(\tilde{C}^\alpha(X; \mathcal{D}_n))] = \infty,$$

where  $\text{Leb}$  denotes the Lebesgue measure.

Conformal inference techniques have been applied to various regression settings, including the estimation of the conditional mean regression function [Lei et al., 2018], conditional quantiles [Sesia and Candès, 2020], and different quantities that arise from conditional distribution functions [Singh et al., 2023, Chernozhukov et al., 2021a]. In recent years, multiple extensions of conformal techniques have emerged to handle counterfactual inference problems [Chernozhukov et al., 2021b, Candès et al., 2023, Yin et al., 2022, Jin et al., 2023], heterogeneous policy effect [Cheng and Yang, 2022], reinforcement learning [Dietterich and Hostetler, ], federated learning [Lu et al., 2023], outlier detection [Bates et al., 2023], hypothesis testing [Hu and Lei, 2023], robust optimization [Johnstone and Cox, 2021], multilevel structures [Fong and Holmes, 2021, Dunn et al., 2022], missing data [Matabuena et al., 2022a, Zaffran et al., 2023], and survival analysis problems [Candès et al., 2023, Teng et al., 2021], as well as problems involving dependent data such as time series and spatial data [Chernozhukov et al., 2021b, Xu and Xie, 2021, Sun, 2022, Xu and Xie, 2023].

Despite the significant progress in conformal inference methods, there has been relatively little work on handling multivariate [Johnstone and Ndiaye, 2022, Messoudi et al., 2022] and functional data [Lei et al., 2013, Diquigiovanni et al., 2022, Matabuena et al., 2021b, Dietterich and Hostetler, 2022, Ghosal and Matabuena, 2023]. In the case of classification problems, the first contributions to handle multivariate responses have also been recently proposed (see, for example, [Cauchois et al., 2021]).

[Zhang and Politis, 2022, Wu and Politis, 2023, Das et al., 2022], provide asymptotic marginal guarantees and, in certain cases, asymptotic results for the conditional coverage. The key idea behind these approaches is the application of resampling techniques, originally proposed by Politis et al. [Politis and Romano, 1994], to residuals or other score measures. Notably, these methodologies are applicable regardless of the predictive algorithm being used, as emphasized by [Politis, 2015].

Bayesian methods are also an important framework to quantify uncertainty (see [Chhikara and Guttman, 1982]), which can also be integrated with conformal inference methods [Angelopoulos and Bates, 2023, Fong and Holmes, 2021, Patel et al., 2023]. Gaussian response theory, including linear Gaussian and multivariate response regression models [Thombs and Schucany, 1990, Li et al., 2022], as a particular case, is a classical and popular approach. However, the latter techniques generally introduce stronger parametric assumptions in statistical modeling or include the limitation or difficulty in selecting the appropriate prior distribution in Bayesian modeling [Gawlikowski et al., 2023]. The theory of tolerance regions gives another connection with the problem studied here [Fraser and Guttman, 1956, Hamada et al., 2004], which was generalized for the multivariate case with the notion of depth bands (see [Li and Liu, 2008]). However, a few conditional depth measures are available in the literature [García-Meixide and Matabuena, 2023]. Depth band measures for statistical objects that take values in metric spaces have recently been proposed [Geenens et al., 2023, Dubey et al., 2022, Liu et al., 2022, Virta, 2023] but only in the unconditional case.

### 1.4.2 Statistical modeling in metric spaces

One of the most prominent applications of statistical modeling in metric spaces is in biomedical problems [Matabuena, 2022]. In personalized and digital medicine applications, it is increasingly common to measure patients' health conditions with complex statistical objects, such as curves and graphs, which allow recording patients' physiological functions and measuring the topological connectivity patterns of the brain at a high resolution level. For example, in recent work, the concept of "glucodensity" [Matabuena et al., 2021a] has been coined, which is a distributional representation of a patient's glucose profile that improves existing methodology in diabetes research [Matabuena et al., 2022a]. This representation is also helpful in obtaining better results with accelerometer data [Matabuena and Petersen, 2023, Ghosal et al., 2021b, Matabuena et al., 2022b, Ghosal and Matabuena, 2023].

From a methodological point of view, statistical regression analysis of response data in metric spaces is a novel research direction [Fan and Müller, 2021, Chen et al., 2021b, Petersen et al., 2021, Zhou and Müller, 2022, Dubey and Müller, 2022, Jeon et al., 2022, Jeon et al., 2022, Kurisu and Otsu, , Chen and Müller, 2023].

The first papers on hypothesis testing [Lyons, 2021, Dubey and Müller, 2019, Petersen et al., 2021, Fout and Fosdick, 2023], variable selection [Tucker et al., 2021], missing data [Matabuena et al., 2024a], multilevel models [Matabuena and Crainiceanu, 2023, Bhattacharjee and Müller, 2023], dimension-reduction [Zhang et al., 2022], semi-parametric regression models [Bhattacharjee and Müller, 2021, Ghosal et al., 2023], semi-supervised algorithms [Qiu et al., 2024] and non-parametric regression models [Schötz, 2021, Hanneke, 2022, Bulté and Sørensen, 2023, Bhattacharjee et al., 2023] have recently appeared.

## 2 Mathematical models

In this section, we present a framework for uncertainty quantification, building upon the previous definition of the oracle prediction region (see Section 1.2):

$$C^\alpha(x) := \mathcal{B}(m(x), r(x)). \quad (15)$$

Recall that  $r(x)$  is the smallest number  $r$  such that  $\mathbb{P}(Y \in \mathcal{B}(m(x), r) \mid X = x) \geq 1 - \alpha$ .

The initial phase of our uncertainty quantification methodology entails the estimation of the Fréchet regression function  $m : \mathcal{X} \rightarrow \mathcal{Y}$ . This estimation process leverages the geometry introduced by the distance function  $d_1$ .

In the second step, we determine the radius that governs the number of points encompassed within the prediction regions. This selection is made to ensure that the set includes at least  $(1 - \alpha)$  proportion of points from the dataset.

We emphasize that our method establishes for different confidence levels  $\alpha \in [0, 1]$ , different level sets for the prediction regions problem. This approach allows us to associate the prediction regions with the notion of conditional quantiles for metric space responses, generalizing the existing marginal approaches [Liu et al., 2022].

### 2.1 Homoscedastic case

Algorithm 1 outlines the core steps of our uncertainty quantification method for the homoscedastic case. The key idea behind our approach is to estimate the function  $m$  and the radius  $r$  by dividing the data into two independent datasets.

In the homoscedastic case, the distribution of  $d_2(Y, m(x))$  remains invariant regardless of the point  $x \in \mathcal{X}$ . As a result, it is natural to which estimate the radius using the empirical distribution from the random sample  $\mathcal{D}_{test} = \{d_2(Y_i, \hat{m}(X_i))\}_{i \in [S_2]}$ . Then, we can formulate a conformalized version of this algorithm to attain non-asymptotic guarantees of the form  $\mathbb{P}(Y \in \tilde{C}^\alpha(X; \mathcal{D}_n)) \geq 1 - \alpha$ .

The core idea of estimating different quantities of the model in different splits is not new in the literature of conformal inference. This approach enhances the computational feasibility of the methods, providing non-asymptotic guarantees and facilitating theoretical asymptotic analysis. However, there may be some loss in statistical efficiency due to estimating model quantities in subsamples. These methods, known as split conformal methods, have been extensively studied (see, for example, [Vovk et al., 2018, Solari and Djordjilović, 2022]).

---

**Algorithm 1** Uncertainty quantification algorithm homoscedastic set-up

---

1. Estimate the function  $m(\cdot)$ , by  $\tilde{m}(\cdot)$  using the random sample  $\mathcal{D}_{train}$ .
  2. For all  $i \in [S_2]$ , evaluate  $\tilde{m}(X_i)$  and define  $\tilde{r}_i = d_2(Y_i, \tilde{m}(X_i))$ .
  3. Estimate the empirical distribution  $\tilde{G}^*(t) = \frac{1}{n_2} \sum_{i \in [S_2]} \mathbb{I}\{\tilde{r}_i \leq t\}$  and denote by  $\tilde{q}_{1-\alpha}$  the empirical quantile of level  $1 - \alpha$  of the empirical distribution function  $\tilde{G}^*(t)$ .
  4. Return  $\tilde{C}^\alpha(x; \mathcal{D}_n) = \mathcal{B}(\tilde{m}(x), \tilde{q}_{1-\alpha})$ .
- 

Observe that we have the marginal finite sample guarantee.

**Proposition 2.** *For any regression function  $m$  and estimator  $\tilde{m}$ , assuming the random elements  $\{(X_i, Y_i)\}_{i=1}^n$  are i.i.d. with respect to a pair  $(X, Y)$ , Algorithm 1 satisfies:*

$$\mathbb{P}(Y \in \tilde{C}^\alpha(X; \mathcal{D}_n)) \geq 1 - \alpha.$$

*Proof.* This follows by observing that

$$\begin{aligned} \mathbb{P}(Y \in \tilde{C}^\alpha(X; \mathcal{D}_n)) &= \mathbb{P}(Y \in \mathcal{B}(\tilde{m}(X), \tilde{q}_{1-\alpha})) \\ &= \mathbb{E}[\mathbb{I}\{d_2(Y, \tilde{m}(X)) \leq \tilde{q}_{1-\alpha}\}] \geq 1 - \alpha. \end{aligned}$$

□

**Remark 1.** *Proposition 2 holds in both the homoscedastic case and the heteroscedastic case. However, when we apply Algorithm 1 to a heteroscedastic model, the resulting conditional coverage can substantially deviate from the true value. Under such circumstances, the algorithm may not be consistency.*

**Remark 2.** *In Algorithm 1, when handling discrete spaces, it becomes crucial to incorporate randomization strategies in the radius estimation. This ensures that the random variable  $d_2(Y, m(X))$  remains continuous, and guarantees that for any two distinct  $\tilde{r}_j$  and  $\tilde{r}_j$ , the probability of them being equal is precisely zero (with probability one).*

*This general strategy has been extensively explored, including [Kuchibhotla, 2020] (see Definition 1), and [Cauchois et al., 2021], which specifically focuses on discrete structures. The integration of randomization techniques in such scenarios ensures the continuity of the random variable and leads to:*

$$1 - \alpha + \frac{1}{n_2 + 1} \geq \mathbb{P}(Y \in \tilde{C}^\alpha(X; \mathcal{D}_n)) \geq 1 - \alpha.$$

### 2.1.1 Statistical consistency theory

Next we introduce the technical assumptions that ensure the asymptotic consistency of the Algorithm 1.

**Assumption 1.** *Suppose that the following hold:*

1.  $n_2 \rightarrow \infty$ .
2.  $\tilde{m}$  is a consistent estimator in the sense that  $\lim_{n_1 \rightarrow \infty} \mathbb{E}(d_2(\tilde{m}(X), m(X)) | \mathcal{D}_{train}) \rightarrow 0$ , in probability.
3. The population quantile  $q_{1-\alpha} = \inf\{t \in \mathbb{R} : G(t) = \mathbb{P}(d_2(Y, m(X)) \leq t) = 1 - \alpha\}$  exists uniquely and is a continuity point of the function  $G(\cdot)$ .

**Theorem 3.** Under Assumption 1, the estimated prediction region  $\tilde{C}^\alpha(x; \mathcal{D}_n)$  obtained using Algorithm 1 satisfies

$$\lim_{n \rightarrow \infty} \mathbb{E}(\varepsilon(\tilde{C}^\alpha(X; \mathcal{D}_n))) \rightarrow 0 \text{ in probability.} \quad (16)$$

*Proof.* See Appendix. □

**Assumption 2.** Suppose that for all  $t \in \mathbb{R}$ , the distribution function of distances  $G(t, x) = \mathbb{P}(d_2(Y, m(x)) \leq t | X = x)$  is uniformly Lipschitz with constant  $L$  in the sense that for all  $t, t' \in \mathbb{R}$  and for all  $x \in \mathcal{X}$ , we have  $|G(t, x) - G(t', x)| \leq L|t - t'|$ .

**Example 3.** Suppose that  $\mathcal{X} = \mathbb{R}^p$ ,  $\mathcal{Y} = \mathbb{R}^m$ ,  $d_1(\cdot, \cdot) = d_2(\cdot, \cdot) = \|\cdot - \cdot\|$  ( $L^2$  norm), and consider the regression model

$$Y = m(X) + \varepsilon, \quad (17)$$

where  $\varepsilon$  is a random vector taking values in  $\mathbb{R}^m$ , and independent from  $X$ . Let  $f$  be the density function of the random variable  $\varepsilon$ . If the density function  $f$  is bounded, then,  $G$  is uniformly Lipschitz.

**Remark 3.** Suppose that the assumptions of Example 3 are satisfied. Consider any estimator  $\tilde{m}$  of  $m$ , and define the distribution of the distances:

$$G^*(t, x) = \mathbb{P}(d_2(Y, \tilde{m}(X)) \leq t | X = x).$$

We can express this probability in terms of the perturbation introduced by the estimator:

$$G^*(t, x) = \mathbb{P}(\|\varepsilon + (m(X) - \tilde{m}(X))\| \leq t | X = x).$$

Then for all  $x$ , the function  $G^*(t, x)$  is Lipschitz continuous with a constant  $L$ .

**Proposition 4.** Under Assumptions 1 and 2, and assuming that  $G^*(t, x) = \mathbb{P}(d_2(Y, \tilde{m}(X)) \leq t | X = x)$ , is uniformly Lipschitz, we can bound the conditional expected error of  $\tilde{C}$  given  $\mathcal{D}_n$  as the sum of two terms: a function of the expected distance between  $\tilde{m}(X)$  and  $m(X)$ , conditional on the training set  $\mathcal{D}_{train}$ , and a function of the difference between the estimated and true  $\alpha$ -quantiles of the distribution of radius  $r$ , denoted by  $\tilde{q}_{1-\alpha}$  and  $q_{1-\alpha}$ , respectively. Specifically, we can write:

$$\mathbb{E}(\varepsilon(\tilde{C}, X) | \mathcal{D}_n) \leq C(\mathbb{E}(d_2(\tilde{m}(X), m(X)) | \mathcal{D}_{train}) + 4(|\tilde{q}_{1-\alpha} - q_{1-\alpha}|)),$$

where  $C$  is a positive constant depending on the Lipschitz constants of the functions  $G$  and  $G^*$ .

*Proof.* See Appendix. □

**Example 4.** Suppose that  $\mathcal{X} = \mathbb{R}^p$ ,  $\mathcal{Y} = \mathbb{R}^m$ , and  $d_1(\cdot, \cdot) = d_2(\cdot, \cdot) = \|\cdot - \cdot\|$  (the  $L^2$  norm). Consider the regression model

$$Y = m(X) + \varepsilon, \quad (18)$$

where  $\varepsilon$  is a random vector taking values in  $\mathbb{R}^m$  and is independent of  $X$ . Let  $f$  denote the density function of  $\varepsilon$ . In the multivariate scale-localization regression models defined in (18), we can obtain the rates of Proposition 4

$$\mathbb{E}(\varepsilon(\tilde{C}, X) | \mathcal{D}_n) \leq C(\mathbb{E}(d_2(\tilde{m}(X), m(X)) | \mathcal{D}_{train}) + 4(|\tilde{q}_{1-\alpha} - q_{1-\alpha}|)).$$

**Remark 4.** *In the absence of covariates and with the Fréchet mean  $m$  known, the rate of our estimation uniquely depends on the speed at which we estimate the quantiles of pseudoresiduals  $r = d(Y, m(X))$ . In this particular homoscedastic case, our bounds extend the optimality results established in [Györfi and Walk, 2019] for the univariate case and empirical distribution, yielding a rate of  $O(\sqrt{\ln n/n})$ . In the case where the Fréchet mean is not known, but we can estimate, it for example at the parametric rate  $O(1/\sqrt{n})$ , our algorithm can exhibit fast rates.*

**Remark 5.** *More specific non-asymptotic results can be derived for homoscedastic cases and univariate responses, as demonstrated in Corollary 1 of [Foygel Barber et al., 2021], using the conformal model introduced in [Lei et al., 2018]. In their work, the authors impose more stringent assumptions to bound the Lebesgue measure, including requirements such as the existence of a density function for the random error and symmetrical conditions, alongside stability criteria for the underlying mean regression functions. In contrast, we do not aim to establish convergence under symmetrical conditions or assume the existence of a density function for the random error. While symmetrical conditions could be relevant in practical applications for obtaining interpretable and valuable regions, they are not imperative from a theoretical perspective within our framework. Moreover, assuming the existence of a density function for the random error is a very strong requirement in many real-world applications.*

**Remark 6.** *In this research, we primarily focus on utilizing our methodology in the setting where  $\mathcal{X} = \mathbb{R}^p$  is a finite-dimensional Euclidean space. However, it is worth noting that our methodology has the potential to be applied when  $\mathcal{X} = \mathbb{H}$ , where  $\mathbb{H}$  is an arbitrary separable metric space with finite diameter under minimal theoretical conditions or a Hilbert space as the case of predictors that lie in a Reproducing Kernel Hilbert Spaces (see for example this representative regression algorithm [Bhattacharjee et al., 2023]). For more details about the statistical models that accommodate such predictors see [Hanneke, 2022]*

## 2.2 Heteroscedastic case

---

**Algorithm 2** Uncertainty quantification algorithm for heteroscedastic setup

---

1. Estimate the function  $\tilde{m}(\cdot)$  using the random sample  $\mathcal{D}_{\text{train}}$ .
  2. For a given new point  $x \in \mathcal{X}$ , let  $X_{(n_2,1)}(x), X_{(n_2,2)}(x), \dots, X_{(n_2,k)}(x)$  denote the  $k$ -nearest neighbors of  $x$  in increasing order based on the distance  $d_2$ . For each data point  $X_i$  in the test dataset  $\mathcal{D}_{\text{test}}$ , compute the predicted value  $\tilde{m}(X_i)$ . Then, define the pseudo-residual  $\tilde{r}_i$  as the distance between the true response value  $Y_i$  and the predicted value  $\tilde{m}(X_i)$ , i.e.,  $\tilde{r}_i = d_2(Y_i, \tilde{m}(X_i))$ . Denote the pseudo-residuals associated with the  $i$ -th ordered observation as  $\tilde{r}_{(n_2,i)}(x) = d_2(Y_{(n_2,i)}, \tilde{m}(x))$ .
  3. Estimate the empirical conditional distribution of order  $1 - \alpha$  by  $\tilde{G}_k^*(x, t) = \frac{1}{k} \sum_{i=1}^k \mathbb{I}\{\tilde{r}_{(n_2,i)}(x) \leq t\}$  and denote by  $\tilde{q}_{1-\alpha}(x)$  the empirical quantile of the empirical distribution  $\tilde{G}_k^*(x, t)$ .
  4. Return the estimated prediction region as  $\tilde{C}^\alpha(x) := \tilde{C}^{\alpha,k}(x) = \mathcal{B}(\tilde{m}(x), \tilde{q}_{1-\alpha}(x))$
- 

The homoscedastic assumption can be too restrictive in metric spaces that lack a linear structure, making a local approach more appropriate. In this paper, we adopt the  $k$ -nearest neighbors (kNN) regression algorithm [Fix and Hodges, 1951, Biau and Devroye, 2015] for this purpose, as it is both computationally efficient and easy to implement.

In heteroscedastic methods, given a point  $x$ , we repeat the same steps as in the homoscedastic algorithm, but the radius estimation only considers data points in a neighborhood of  $x$ , denoted as  $N_k(x) = \{i \in [S_2] :$

$d_2(X_i, x) \leq d_{2(n_2, k)}(x)$ . Here,  $d_{2(n_2, k)}(x)$  represents the distance between  $x$  and its  $k$ -th nearest neighbor in increasing order in the test dataset  $\mathcal{D}_{\text{test}}$  using the distance  $d_2$ . Algorithm 2 provides a detailed outline of this procedure.

**Remark 7.** *Although Algorithm 2 can be consistent, it lacks finite sample guarantees. To address this limitation and propose a heteroscedastic algorithm with non-asymptotic performance guarantees, we suggest extending the conformal quantile methodology introduced by [Romano et al., 2019] to our context. Specifically, we aim to achieve the marginal property  $\mathbb{P}(Y \in \tilde{C}^\alpha(X; \mathcal{D}_n)) \geq 1 - \alpha$ . The core steps are outlined below:*

1. **Estimation of  $m(\cdot)$ :** Utilize the dataset  $\mathcal{D}_{\text{train}}$  to estimate the regression function  $m(\cdot)$ .
2. **Estimation of  $r(\cdot)$ :** Employ the random sample  $\mathcal{D}_{\text{test}}$  and the pairs  $(X_i, d_2(Y_i, \tilde{m}(X_i)))$  for each  $i \in [S_2]$  to estimate the radius function  $r(\cdot)$ .
3. **Calibration of  $\tilde{r}(x)$ :** In an additional data-split  $\mathcal{D}_{\text{test}2}$ , we calibrate the radius  $\tilde{r}(x)$  to obtain the non-asymptotic guarantees using the scores  $S_i = d_2(Y_i, \tilde{m}(X_i)) - \tilde{r}(X_i)$ . The empirical quantile at level  $\alpha$ , denoted by  $\tilde{w}_\alpha$ , is then used to define the final radius function as  $\hat{r}(x) = \tilde{r}(x) + \tilde{w}_\alpha$ .

### 2.2.1 Statistical Theory

The following technical assumptions are introduced to guarantee that the proposed heteroscedastic  $k$ NN-algorithm is asymptotically consistent.

**Assumption 3.** 1.  $n_2 \rightarrow \infty$ .

2.  $\tilde{m}$  is a consistent estimator in the sense that  $\mathbb{E}(d_2(\tilde{m}(X), m(X)) | \mathcal{D}_{\text{train}}) \rightarrow 0$  in probability as  $n_1 \rightarrow \infty$ .
3. As  $n_2 \rightarrow \infty, k \rightarrow \infty$ , and  $\frac{k}{n_2} \rightarrow 0$ .
4. Except in a set of probability zero, for all  $x \in \mathcal{X}$ , the pointwise population quantile  $q_{1-\alpha}(x) = \inf\{t \in \mathbb{R} : G(t, x) = \mathbb{P}(d_2(Y, m(x)) \leq t | X = x) = 1 - \alpha\}$  exists uniquely and is a continuity point of the function  $G(\cdot, x)$ .
5. Except in a set of probability zero, for all  $x \in \mathcal{X}$ ,  $\mathbb{E}(d_2(Y, m(x)) | X = x) < \infty$ .

**Theorem 5.** Under Assumption 3, the uncertainty quantification estimator  $\tilde{C}^{\alpha, k}(\cdot)$  obtained using Algorithm 2 satisfies:

$$\lim_{n \rightarrow \infty} \mathbb{E}(\varepsilon(\tilde{C}, X) | \mathcal{D}_n) \rightarrow 0.$$

*Proof.* The proof is given in the Appendix. □

**Remark 8.** We can generalize Proposition 4 using Assumption 3 for the  $k$ NN algorithm (and introducing another modified Lipschitz condition for the radius estimation  $r = d_2(Y, m(X))$ , see [Györfi and Walk, 2019]):

$$\mathbb{E}(\varepsilon(\tilde{C}, X) | \mathcal{D}_n) \leq C(\mathbb{E}(d_2(\tilde{m}(X), m(X)) | \mathcal{D}_{\text{train}}) + 4(\mathbb{E}(|\tilde{q}_{1-\alpha}(X) - q_{1-\alpha}(X)|))).$$

In the heteroscedastic case, we must consider explicitly the impact of the conditional quantile  $q_{1-\alpha}(x)$  for each  $x \in \mathcal{X}$  in the rate. In a similar context, Györfi et al. [Györfi and Walk, 2019] propose the optimal rate for prediction intervals, which coincides when the conditional regression function  $m$  is known and is given by  $O\left(\frac{\ln n}{n^{\frac{1}{p+2}}}\right)$  for  $p \geq 1$ , where  $p$  denotes the dimension of the predictor  $X$ . It is important to note that this rate scales with the dimension of the covariate space  $p$ , unlike the homoscedastic or non-covariate settings.

## 2.3 Global Fréchet regression model

In this section, we introduce some background on regression modeling in metric spaces, which is essential for implementing our uncertainty quantification algorithms in practice. After motivating the need for models that handle random responses in metric spaces, particularly in clinical applications, the primary objective of this section is to introduce the global Fréchet regression model. This regression model in metric spaces will be employed across various analytical tasks.

The goal is to model the regression function

$$m(x) = \operatorname{argmin}_{y \in \mathcal{Y}} \mathbb{E}(d_1^2(Y, y) | X = x)$$

so that its estimation becomes feasible.

In this section, we focus on a specific regression model designed for metric-space valued outcomes, known as the *global Fréchet regression model* [Petersen and Müller, 2019].

The global Fréchet regression model provides a natural extension of the standard linear regression model from Euclidean spaces to metric spaces.

Our interest in this model stems from its potential applications in the field of medical data analysis. As medical technology continues to advance, we expect to have access to increasing amounts of complex data about patients' health conditions.

To illustrate the significance of uncertainty quantification in this context, we turn our attention to the continuous glucose monitoring technology. Consider two non-diabetic individuals who share identical clinical characteristics, except for their body mass index. Our primary focus is to predict their glucose quantile functions. As depicted in Figure 1, both individuals exhibit the same conditional mean function (indicated by the black line). However, it is important to note that the uncertainty in the prediction curves increases with higher body mass.

In practical terms, if we were to use the conditional mean results to modify the diet based on changes in the glucose profiles of overweight patients, we would encounter technical difficulties. The patient responses in this subgroup turn out to be heterogeneous and individualized responses, as evidenced by the varying levels of uncertainty in the predictions. As a consequence, relying solely on prescriptive data-driven algorithms based on conditional mean regression function would prove inadequate for optimizing diet selection among these patients.

To effectively utilize uncertainty quantification algorithms, we consider the global Fréchet model, a generalization of linear regression to metric-space valued responses.

In particular, [Petersen and Müller, 2019] propose to model the regression function in the form

$$m(x) = \operatorname{argmin}_{y \in \mathbb{R}} \mathbb{E} [\omega(x, X) d(Y, y)^2] ,$$

where the weight function  $\omega$  is defined by

$$\omega(x, z) = 1 + (z - \mu)^\top \Sigma^{-1} (x - \mu)$$

with  $\mu = \mathbb{E}(X)$  and  $\Sigma = \operatorname{Cov}(X)$ . As [Petersen and Müller, 2019] show, in the case of  $\mathcal{Y} = \mathbb{R}$ , this model reduces to standard linear regression.

While in our applications we primarily focus on developing estimators in the global Fréchet regression model, it is important to emphasize that our uncertainty quantification algorithm can be applied to any regression technique, including random forests in metric spaces. It should be noted, however, that if the global Fréchet models do not align with the conditional Fréchet mean  $m$ , the resulting estimators will be inconsistent.

To estimate the conditional mean function  $m(x)$  under the global Fréchet model from a random sample  $\mathcal{D}_n = \{(X_i, Y_i)\}_{i=1}^n$ , we may solve the counterpart empirical problem

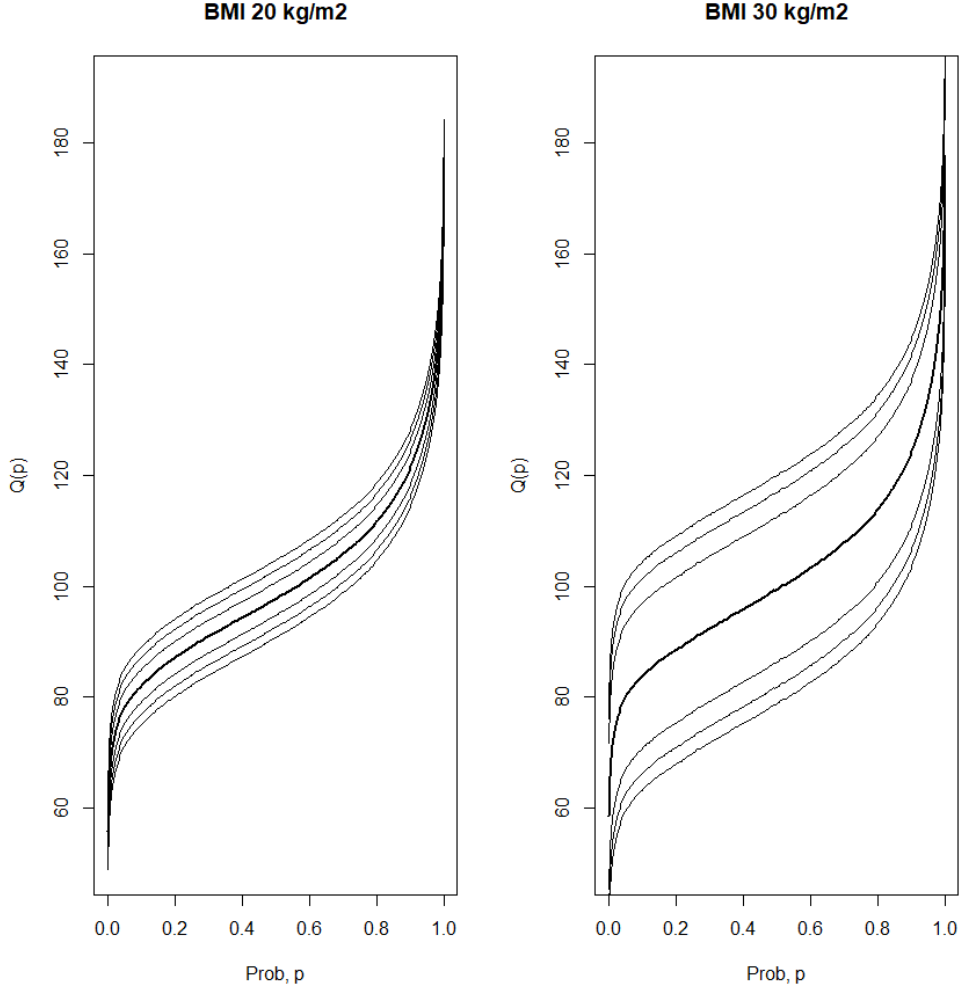


Figure 1: Uncertainty quantification from the quantile glucose representations for two non-diabetic patients with the same clinical characteristics, with the exception of body mass index (BMI). In patient (i),  $BMI = 20\text{kg/m}^2$ , and in patient (ii),  $BMI = 30\text{kg/m}^2$  (more uncertainty).

$$\tilde{m}(x) = \operatorname{argmin}_{y \in \mathcal{Y}} \frac{1}{n} \sum_{i=1}^n [\omega_{in}(x) d_1^2(y, Y_i)], \quad (19)$$

where  $\omega_{in}(x) = \left[ 1 + (X_i - \bar{X}) \tilde{\Sigma}^{-1} (x - \bar{X}) \right]$ , with  $\bar{X} = \frac{1}{n} \sum_{i=1}^n X_i$ , and  $\tilde{\Sigma} = \frac{1}{n-1} \sum_{i=1}^n (X_i - \bar{X})(X_i - \bar{X})^\top$

## 2.4 Testing Homoscedastic and Heteroscedastic Nature of the Uncertainty Quantification Model

In this section, we introduce rigorous criteria for testing whether the distribution  $(X, Y)$  is homoscedastic.

From a practical standpoint, model users are faced with a choice between employing the homoscedastic or heteroscedastic algorithm. In the former case, finite sample guarantees are available, whereas in the latter case, only consistency guarantees exist. If the underlying distributional model is not homoscedastic and we use such an algorithm, the estimated conditional predictions regions would be inconsistent. From a mathematical statistical perspective, the appropriate criterion for deciding which model to choose is to test the null hypothesis that, for all  $x \in \mathcal{X}$ , and  $r \geq 0$ :

$$\mathbb{P}(Y \in \mathcal{B}(m(x), r) \mid X = x) \quad (20)$$

is independent of  $x$ .

Alternatively, we can define the problem as to test that the random variable of the pseudo-residuals  $r = d_2(Y, m(X))$  is independent of  $X$ , i.e.,  $H_0 : r \perp X$  versus  $H_a : r \not\perp X$ .

To achieve this, we first estimate the regression function  $m$  using the random elements of  $\mathcal{D}_{\text{train}}$ , obtaining an estimator  $\tilde{m}$ . Subsequently, we construct a hypothesis test with the random sample  $\mathcal{D}_{\text{test}} = \{X_i, d_2(Y_i, \tilde{m}(X_i))\}_{i \in [S_2]}$ . Due to the structural hypothesis, as  $\tilde{m}$  is a consistent estimator, meaning that  $\mathbb{E}(d_2(\tilde{m}(X), m(X)) \mid \mathcal{D}_{\text{train}}) \rightarrow 0$  in probability as  $|\mathcal{D}_{\text{train}}| \rightarrow \infty$ , it is expected, that hypothesis testing for homoscedasticity is consistent.

In this article, we propose employing an existing multivariate independence testing methodology—distance covariance or distance correlation (the standardized version) [Székely et al., 2007b, Zhong et al., 2023]—as a formal criterion for testing the homoscedasticity of  $(X, Y)$  with respect to the regression function  $m$ . This builds upon the original hypothesis testing framework of homoscedasticity from [Goldfeld and Quandt, 1965] for univariate responses. Our approach is methodologically valid for testing the homoscedastic nature of the pair  $(X, Y)$  when the predictor  $X$  takes values in separable Hilbert spaces [Lyons, 2013].

Let us start with the definition of the sample distance covariance for the Euclidean distance  $\|\cdot - \cdot\|$ .

For all  $i \in [S_2]$ , consider the bivariate random element  $(X_i, d_2(Y_i, \tilde{m}(X_i)))$ .

**Definition 4.** *The squared sample distance covariance (a scalar) is the arithmetic average of the products  $A_{j,k} \cdot B_{j,k}$ :*

$$\widetilde{\text{dCov}}^2(X, r) = \frac{1}{n_2^2} \sum_{j \in [S_2]} \sum_{k \in [S_2]} A_{j,k} \cdot B_{j,k},$$

where

$$\begin{aligned} A_{j,k} &= a_{j,k} - \bar{a}_j - \bar{a}_k + \bar{a}.. & j, k \in [S_2], \\ B_{j,k} &= b_{j,k} - \bar{b}_j - \bar{b}_k + \bar{b}.. & j, k \in [S_2] \end{aligned}$$

with

$$\begin{aligned} a_{j,k} &= \|X_j - X_k\|, & j, k \in [S_2], \\ b_{j,k} &= \|d_2(Y_j, \tilde{m}(X_j)) - d_2(Y_k, \tilde{m}(X_k))\|, & j, k \in [S_2], \end{aligned}$$

and  $\bar{a}_j$  is the  $j$ -th row mean,  $\bar{a}_k$  is the  $k$ -th column mean, and  $\bar{a}..$  is the grand mean of the distance matrix of the  $X$  sample. The notation is similar for the  $b$  values.  $\|\cdot\|$  denotes the Euclidean norm.

The following consistency result enables us to develop a consistent hypothesis test to determine whether the random pair  $(X, Y)$  exhibits homoscedasticity with respect to the function  $m$ .

**Proposition 6.** *Suppose that  $\mathbb{E}(\|X\|) < \infty$ ,  $\mathbb{E}(r) < \infty$ , and  $\mathbb{E}(d_2(\tilde{m}(X), m(X)) \mid \mathcal{D}_{\text{train}}) \rightarrow 0$  in probability as  $|\mathcal{D}_{\text{train}}| \rightarrow \infty$ . Then*

$$\lim_{n_1 \rightarrow \infty} \lim_{n_2 \rightarrow \infty} \widetilde{\text{dCov}}^2(X, r) = \text{dCov}^2(X, r), \quad (21)$$

where  $\text{dCov}(X, r)$  is the population definition of the distance covariance introduced in [Székely et al., 2007b].

*Proof.* Theorem 2 from [Székely et al., 2007b] using the hypothesis  $\mathbb{E}(d_2(\tilde{m}(X), m(X)) | \mathcal{D}_{\text{train}}) \rightarrow 0$  in probability as  $|\mathcal{D}_{\text{train}}| \rightarrow \infty$ .  $\square$

Then, the test statistic  $T_{n_2} = n_2 \widetilde{\text{dCov}}^2(X, r)$  determines a statistical tests asymptotically valid to any deviation (alternative) from the null hypothesis. For an implementation, see the `dcov.test` function in the `energy` package for R.

From a practical perspective, we provide several alternatives to calibrate the test statistics under the null hypothesis and derive  $p$ -values, including permutation methods, resampling methods based on Efron's Naive bootstrap, or the Wild bootstrap [Székely et al., 2007b, Matabuena et al., 2022a, Matabuena et al., 2023b]. Each of these calibration options offers valuable means to fine tune the statistical tests, for diverse analysis requirements.

## 2.5 New model constructions: variable selection methods for regression models in metric spaces

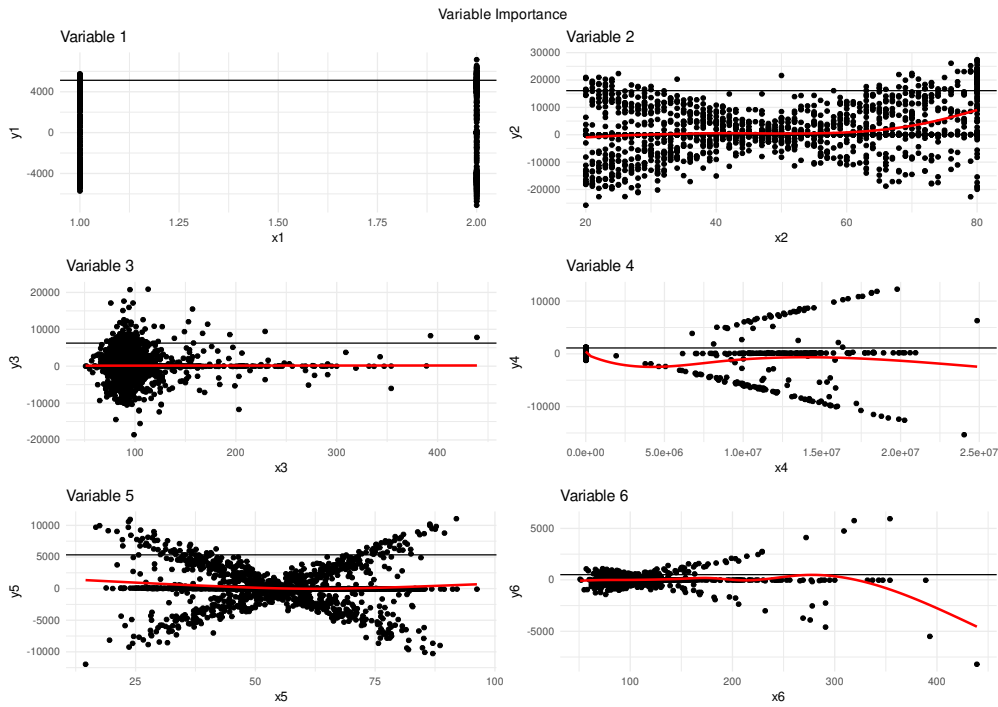


Figure 2: An example of the new local variable model, including six predictors. The first predictor is a binary variable representing the individual's sex, and the remaining variables are continuous biomarkers. Based on the results obtained, all variables except for variables 3 and 5 were found to be important globally in this example.

In this section, we present a variable selection model that can be applied to any arbitrary regression models operating within metric spaces. Before we begin, it is important to clarify that we utilize uncertainty quantification algorithms applied over a transformed random variable  $W$  on the real line, then we can apply over traditional conformal inference techniques. The critical modeling step is to combine the different steps of our uncertainty algorithms to create a variable selection algorithm using scalar methods. For simplicity, we consider that the underlying regression function  $m$  is defined through the global Fréchet Regression model

$$m(x) = \operatorname{argmin}_{y \in \mathcal{Y}} \mathbb{E} [\omega(x, X) d_1^2(Y, y)], \quad (22)$$

where  $\Sigma$  is the covariance matrix of  $X$ ,  $\mu = \mathbb{E}(X)$ ,  $\omega(x, X) = [1 + (X - \mu)\Sigma^{-1}(x - \mu)]$ .

Let  $m(\cdot)$  denote the regression function with the  $p$ -covariates and  $m_{-j}(\cdot)$  denote the regression function obtained by excluding the  $j$ th variable from the model. To evaluate the relevance of the  $j$ th predictor, we introduce the random variable  $W(X, Y) = d_1^2(Y, m_{-j}(X)) - d_1^2(Y, m(X))$  such that  $\mathbb{E}(W(X, Y)) \leq 0$ . From a theoretical point of view, under the null hypothesis,  $H_0 : j \in \{1, \dots, p\}$  is an irrelevant predictor, the random variable  $W(X, Y)$  is equal to zero with probability one. In order to test this null hypothesis, we construct a univariate prediction interval following the methodology established in Sections 2.1 and 2.2 respectively (for  $\mathcal{Y} = \mathbb{R}$ ), denoted as  $\tilde{C}^\alpha(X)$ , where  $\mathbb{P}(W(X, Y) \in \tilde{C}^\alpha(X)) \geq 1 - \alpha$ , and we check if this interval contains only positive values. This hypothesis can be tested locally and globally for a pre-specified confidence level  $\alpha \in [0, 1]$ .

The new variable selection method offers several significant advantages over existing variable selection methods in metric spaces [Tucker et al., 2021]. Firstly, it provides a local measure of the importance of the  $j$ th variable, as demonstrated in Figure 2. Unlike its competitors, our method can be applied in more general settings beyond linear models, including additive or semiparametric models [Lin et al., 2023], and it effectively handles categorical predictors (with two or more levels as group-Lasso models [Wang and Leng, 2008]). Notably, the existing variable selection methods for metric space responses [Tucker et al., 2021] inform about the global importance of the  $j$ th predictor, while our approach is local, being more flexible and informative about the contribution of a predictor in a specific region of the prediction space.

Secondly, our method does not necessitate variable standardization, making it more practical and straightforward to use. Additionally, it provides a  $p$ -value that reflects the strength of each variable, enabling an assessment of their significance.

To obtain a global  $p$ -value indicating the significance of each variable, we introduce an additional notation. We define the functions  $\tilde{W}_j(x, y) = d_1^2(y, \tilde{m}_{-j}(x)) - d_1^2(y, \tilde{m}(x))$  and consider the median or integrated median computed from the random elements of the sample  $\mathcal{D}_{\text{test}}$ . For instance, we calculate  $\tilde{w}_j = \frac{1}{|\mathcal{D}_{\text{test}}|} \sum_{i \in \mathcal{D}_{\text{test}}} \tilde{W}_j(X_i, Y_i)$  and employ a  $t$ -test to evaluate the null hypothesis  $H_0 : w_j \leq 0$  against  $H_a : w_j > 0$ . Alternatively, a Wilcoxon test can be used, which tends to be more robust in the presence of outliers. In this paper, we employ a Wilcoxon test to assess the significance of each variable and apply a Bonferroni correction to adjust the confidence level for multiple comparisons. Along this paper, we implement this variable selection procedure with the homoscedastic algorithm defined in Section 2.1.

### 3 Simulation study

We conducted a comprehensive simulation study to rigorously evaluate the empirical performance of the proposed uncertainty quantification framework with finite samples. The study encompassed a wide range of scenarios and diverse data structures.

### 3.1 Multidimensional Euclidean data

#### 3.1.1 Homoscedastic case

To evaluate the methods performance under homoscedastic conditions and controlled settings, we conducted a simulation study based on the classical multivariate Gaussian linear regression model. Specifically, we consider a  $p$ -dimensional Gaussian predictor variable  $X = (X_1, \dots, X_p)^\top \sim \mathcal{N}((0, \dots, 0)^\top, \Sigma)$ , where  $(\Sigma)_{ij} = \rho \in [0, 1]$  for all  $i \neq j$  and  $(\Sigma)_{ii} = 1$  for all  $i = 1, \dots, p$ . Additionally, we consider an  $s$ -dimensional random response variable  $Y = (Y_1, \dots, Y_s)^\top \in \mathbb{R}^s$ , modeled by the functional relationship:

$$Y = m(X) + \varepsilon = X^\top \beta + \varepsilon, \quad (23)$$

where  $\beta$  is a  $p \times s$  matrix of coefficients with all entries equal to 1. The random error  $\varepsilon = (\varepsilon_1, \dots, \varepsilon_s)^\top \sim \mathcal{N}(0, \text{diag}(1, \dots, 1))$  is assumed to be independent from  $X$  and satisfies  $\mathbb{E}(\varepsilon|X) = 0$ .

To assess the performance of our methods under various scenarios, we conducted a comprehensive simulation study with multiple cases. We explored different configurations for the values of  $s$  and  $p$ , as well as various sample sizes, confidence levels, and correlation structures for the covariance matrix  $\Sigma$ , governed by the parameter  $r \in [0, 1]$ . Specifically, we considered  $s \in \{1, 2, 5\}$  and  $p \in \{1, 2, 5, 10\}$ , while the sample size  $n$  varied between 500 and 5000 data points. The confidence levels  $\alpha$  ranged from 0.05 to 0.5, and we set correlation parameters  $r$  equal to 0, 0.2, 0.4, and 0.6. Here, we only show the results in an intermediate range with  $s = 2$ ,  $p = 0.5$ ,  $r = 0.2$ , and  $n \in \{500, 1000, 5000\}$ .

To ensure the robustness of our findings, we employed a training set of size  $|\mathcal{D}_{train}| = n/2$  and a test set of size  $|\mathcal{D}_{test}| = n - |\mathcal{D}_{train}|$ . Each scenario was repeated 500 times, and we evaluated the finite marginal coverage in an additional test set  $|\mathcal{D}_{test2}| = 5000$  drawn from the same probability law.

For estimation purposes, we obtained estimates of the regression function  $m$  using a multivariate response linear regression model with the standard mean square criteria [Seber and Lee, 2003]. Subsequently, we applied Algorithm 1, as defined in Section 2.1, to generate prediction regions. The results for various confidence levels and sample sizes are illustrated in Figure 3. It is evident that the algorithm consistently maintains the desired marginal coverage, and as the sample size increases, the variability decreases. This observation indicates the good performance of our algorithm across diverse scenarios, in accordance with its non-asymptotic guarantees and theoretical consistency properties.

#### 3.1.2 Heteroscedastic case

To account for heteroscedasticity in the simulation scenarios, we modify the previous simulation scheme and incorporate an additional term  $\sigma : \mathbb{R}^p \rightarrow \mathbb{R}$  that represents the heteroscedastic term in the model. Specifically, we set the random error term to be  $\sigma(X)\varepsilon$ , where  $\sigma(x) = \|x\|_2$  is a function that maps each feature vector to a scalar value corresponding to their norm. The overall generative model we consider is:

$$Y = m(X) + \sigma(X)\varepsilon = X^\top \beta + \|X\|_2 \varepsilon, \quad (24)$$

To estimate the regression function, we use linear regression without incorporating the heteroscedastic covariance structure in the model estimation. Although this estimator is not the most efficient in the sense of the Gauss-Markov theorem [Harville, 1976], which deals with unbiased and minimum variance characters, the estimator remains consistent.

In this case, we use the algorithm presented in Section 2.2, denoted as Algorithm ??, and utilize the  $k$ -nearest neighbor (kNN) algorithm with varying values of  $k$ :  $k = 10, 20, 50$ , and 100. We evaluate the marginal coverage of the resulting predictions to assess the accuracy of the model. The results of our analysis are presented in Figure 4, following a format similar to the previous example. This figure offers insights into our methods performance across various values of  $k$  and assists in determining the optimal choice of  $k$ . The selection of this optimal value is guided by specific uncertainty quantification results,

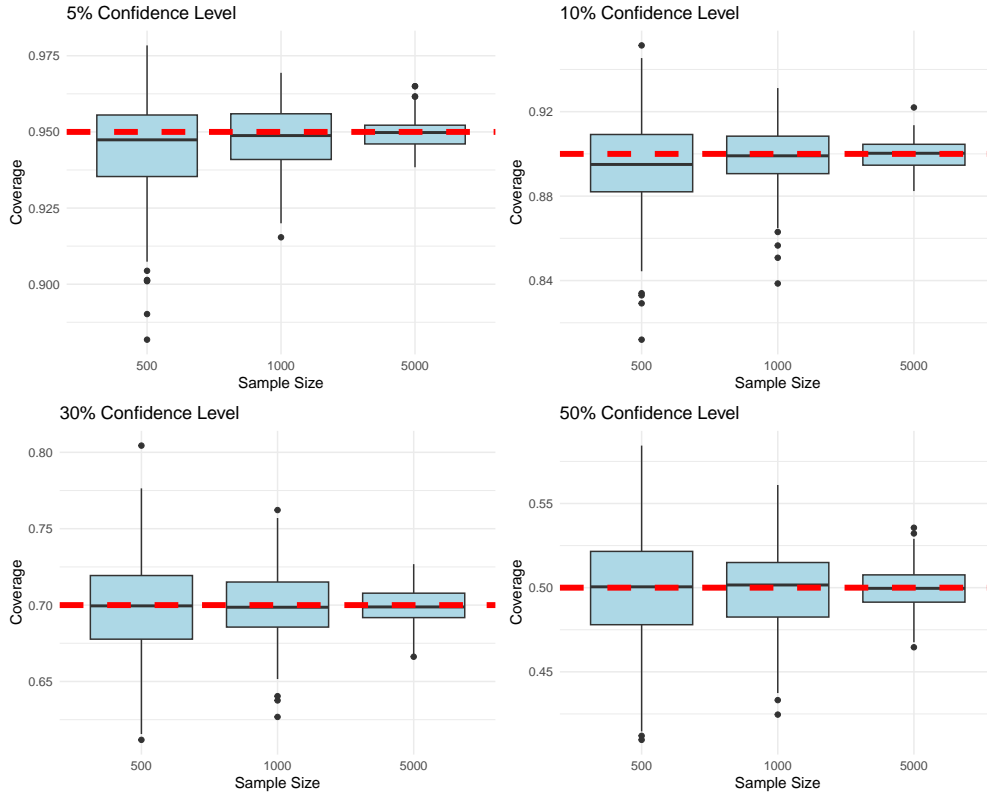


Figure 3: The figure shows the distribution of the marginal coverage  $\mathbf{P}(Y \in \tilde{C}^\alpha(X))$  in the homoscedastic case across different sample sizes and confidence levels. The results of our analysis provide insights into how the marginal coverage varies as a function of sample size and confidence level.

which are tailored to the characteristics of the dataset and the coverage achieved during the analysis of the results.

The analysis of empirical results highlights the sensitivity of the method's performance to the choice of the parameter  $k$ , especially when dealing with small confidence levels and situations where multiple neighbors are required to approximate extreme quantiles. Across various dimensions of the response variable and predictors, we see that the method maintains stable performance as the sample size increases. However, it is important to acknowledge that in the heteroscedastic case, tuning the  $k$  parameter on a case-by-case basis may be necessary. We are well aware, both from empirical evidence regarding the use of  $k$ -nearest neighbors (kNN) for estimating conditional means and theoretical results, that the choice of the smoothing parameter  $k$  is of utmost importance in achieving estimators with good empirical properties (see [Zhang et al., 2018]).

Lastly, we must note that at a median level corresponding to  $\alpha$  parameter of 0.5, the marginal coverage is consistent across different situations examined, demonstrating the robustness of the method in detecting prediction regions that contain half of the sample.

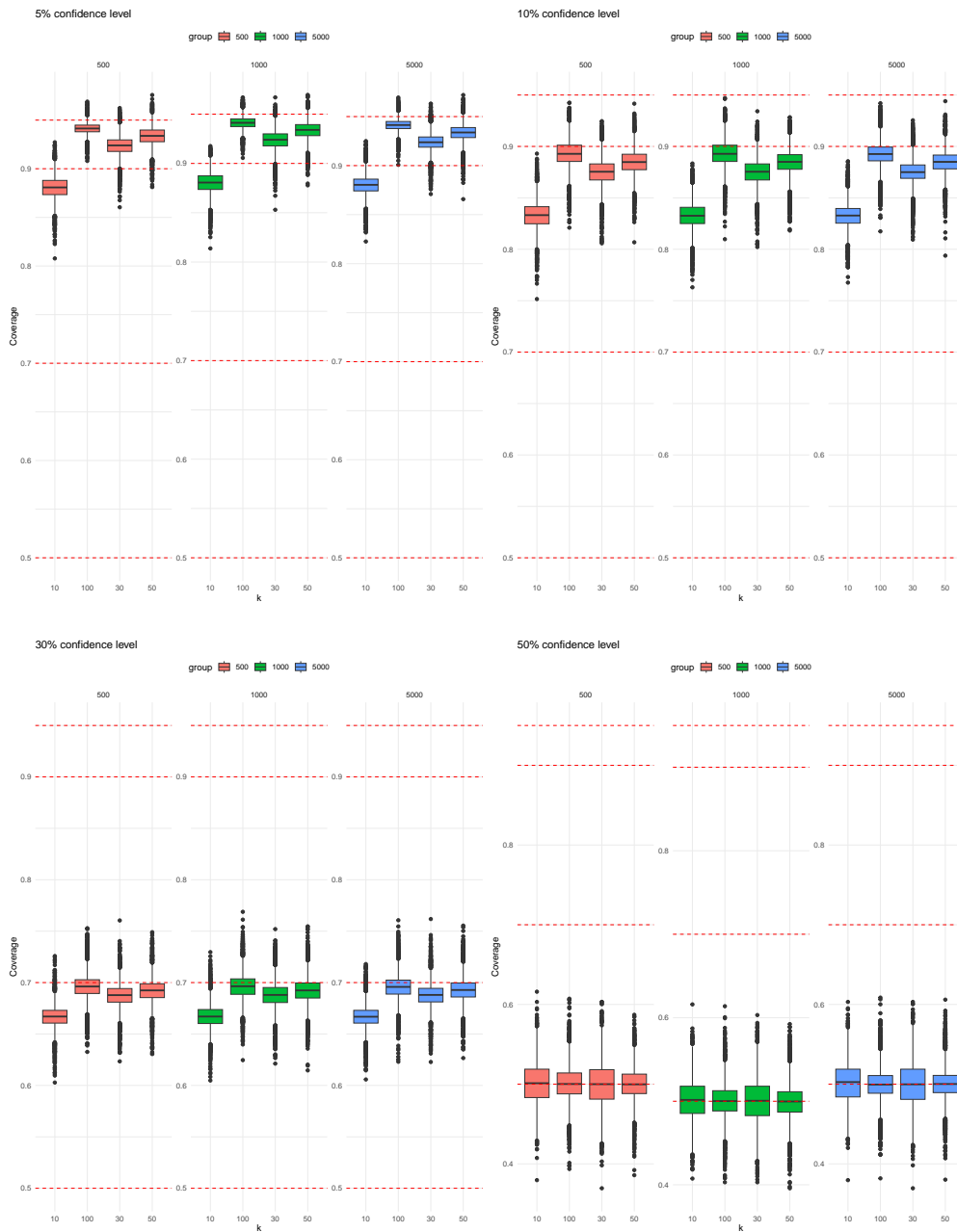


Figure 4: The figure illustrates how the distribution of the marginal coverage  $\mathbf{P}(Y \in \tilde{C}^\alpha(X))$  in the heterocedastic case varies across different sample sizes and confidence levels as the number of neighbors changes. Our results provide insights into the behavior of the marginal coverage and the impact of the number of neighbors on the performance of our method.

## 3.2 Examples of probability distribution

### 3.2.1 Uncertainty quantification

Let us revisit Example 2 from the introduction, where we develop a model to represent observations drawn from a latent continuous process by utilizing their distribution function. Formally, we define the spaces  $\mathcal{X} = \mathbb{R}^p$  and  $\mathcal{Y} = \mathcal{W}_2(\mathbb{R})$ . Here,  $\mathcal{W}_2(\mathbb{R})$  represents the 2-Wasserstein space, equipped with the 2-Wasserstein metric  $d_{\mathcal{W}_2}^2(F, G) = \int_0^1 (Q_F(t) - Q_G(t))^2 dt$ .  $Q_F$  and  $Q_G$  denote the quantile functions of the distribution functions  $F$  and  $G$ , respectively.

For our specific simulation purposes, we suppose that the underlying generative model is defined:

$$Z(j) = 100 + 5 \cdot \sum_{l=1}^p X_l + \varepsilon(j), \quad j = 1, \dots, n.$$

Let

$$\tilde{F}(\rho) = \frac{1}{n} \sum_{j=1}^n \mathbb{I}\{Z(j) \leq \rho\}. \quad (25)$$

We set  $n = 300$ . The remaining parameters are established as in the previous simulations related to the multivariate Euclidean data, with  $p = 5$  and  $n_i$  ranging from 500 to 5000. We use a training set of size  $|\mathcal{D}_{\text{train}}| = n/2$  and a test set of size  $|\mathcal{D}_{\text{test}}| = n - |\mathcal{D}_{\text{train}}|$ , and repeat each scenario 500 times, evaluating the finite marginal coverage at additional test points  $|\mathcal{D}_{\text{test2}}| = 5000$  using the same probability law as the pair  $(X, Z)$ .

For estimation purposes, we utilize the Global-Fréchet model equipped with the 2-Wasserstein distance to predict the quantile response variable. We consider the Euclidean distance, denoted as  $d_2$ , between the predicted quantiles and the observed estimated quantile function. The confidence level  $\alpha$  is fixed with values varying from 0.05 to 0.5. It is important to note that in our example, we use estimated quantile functions from a time series as the response variable, introducing additional sources of uncertainty and making it challenging to obtain exact marginal control. Despite this, the underlying model follows a homoscedastic definition introduced in Section 1.2. The results, presented in figure 5, confirm this hypothesis and indicate that the obtained coverage is anti-conservative (below the nominal value) but very close to the real nominal values. Again, we note that at a median level corresponding to  $\alpha = 0.5$ , the marginal coverage is consistent across different situations examined, demonstrating the robustness of the method in detecting prediction regions that contain half of the sample.

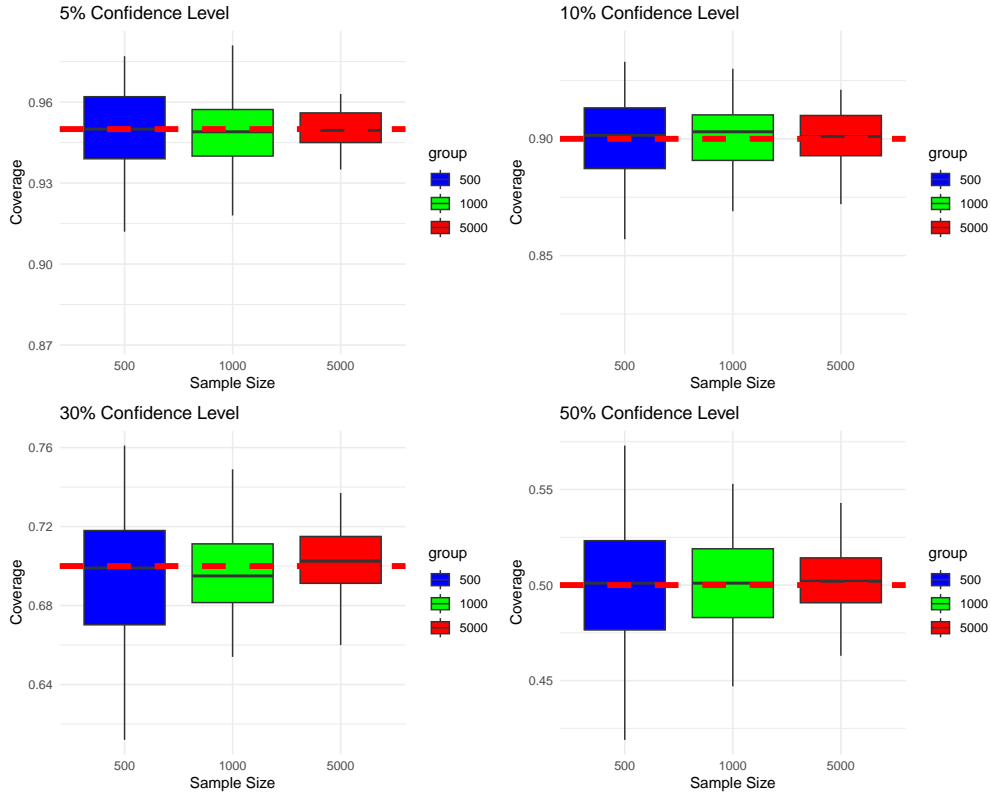


Figure 5: The figure presents the distribution of the marginal coverage across different confidence levels and sample sizes in the distributional data analysis example. The analysis utilized estimated quantile functions from a time series as the response variable, introducing additional sources of variability and making it challenging to obtain exact marginal control, despite the underlying regression model being homoscedastic. Nonetheless, the results indicate that the method is effective in obtaining conservative coverage levels that are very close to the true values.

### 3.2.2 Variable selection

Continuing with the previous example, we now consider the case where the number of variables that appear in the generative model is equal to  $p_{\text{true}} = 1$  (the first covariate for simplicity) across all scenarios. For each  $j = 1, \dots, n$ , the specific generative model is given by

$$Z(j) = 100 + 5 \cdot X_1 + \varepsilon(j).$$

To identify the most relevant variable for the model, we employ the variable selection strategies outlined in Section 2.5, with a confidence level of  $\alpha = 0.05$ . For this purpose, we utilize the Global-Fréchet regression model as a base regression model to predict the empirical quantile function.

An important point in the variable selection modeling strategy, highlighted in Section 2.5, is that we are testing simultaneously  $p$ -hypotheses, and we must address the statistical problems of multiple comparisons. In this paper, we implement the Bonferroni method for multiple comparisons. Table 1 displays the results across different sample sizes, demonstrating the statistical consistency of the variable selection approach as the sample size increases in this example.

	Detect True Variables (%)	One Variable False Positive (%)	Two or More Variables False Positive (%)
$n = 500$	100	68	26
$n = 1000$	100	29	4
$n = 5000$	100	3	1

Table 1: Results of Simulations for Variable Selection Approach

## 4 Data analysis examples

In this section, we demonstrate the wide-ranging utility and adaptability of our algorithm across different data structures and statistical modeling scenarios through a series of real-world examples. Our emphasis is on showcasing the algorithm’s applicability in modern medical contexts.

The initial example explores situations lacking predictors, utilizing insights from shape analysis to characterize Parkinson’s disease using digital biomarkers. This contrasts with the next four examples, which examine pairs  $(X, Y) \in \mathcal{X} \times \mathcal{Y}$ , offering a broader perspective on the algorithm’s performance in regression analyses.

### 4.1 Shape Analysis

#### 4.1.1 Motivation

Shape analysis is a research area that requires novel statistical methods in metric spaces [Dryden and Mardia, 2016, Steyer et al., 2023] and has broad applications in the biomedical sciences. This approach is particularly useful when analyzing random objects based on their geometrical properties. Here, we are motivated to analyze the shapes of handwritten samples from patients with a neurological disorder versus those from a control group of healthy individuals. The scientific problem we aim to address in this section is to define uncertainty prediction regions for healthy individuals at some confidence level  $\alpha \in (0, 1)$ , using handwriting trajectories. Assuming that individuals with the neurological disorder exhibit behaviors that deviate significantly from those expected of the control group in their writing shapes. We use these prediction regions to identify patients who differ markedly from the control group and to detect and characterize outlier behavior.

#### 4.1.2 Data Description

This study employs data from [Isenkul et al., 2014], comprising  $n_1 = 15$  control subjects and  $n_2 = 30$  individuals diagnosed with Parkinson’s disease, to analyze handwriting shapes captured through digital tests. Our objective is to establish expected prediction regions at different confidence levels  $\alpha$  based on the control group’s data. For this purpose, first we estimate the empirical Fréchet mean using Euclidean distance  $d_1^2(\cdot, \cdot) = \|\cdot - \cdot\|^2$ . Subsequently, we adopt  $d_2(\cdot, \cdot) = \|\cdot - \cdot\|_\infty$  to graphically represent the tolerance regions for various individuals across confidence levels, utilizing the convex hull of extreme points for visualization purposes.

#### 4.1.3 Results

Figure 6 illustrates the handwriting trajectories alongside tolerance regions for confidence levels  $\alpha = 0.5$  and  $\alpha = 0.7$ , including those from individuals with Parkinson’s disease (yellow color). For individuals affected by Parkinson’s, employing tolerance regions at  $\alpha = 0.5$  enables distinguishing over 75% of the

patients by examining whether their handwriting shape falls within or outside these predefined regions. These findings are encouraging, showcasing the potential of our uncertainty quantification approach in validating novel digital biomarkers for contemporary medical applications, such as analyzing handwriting patterns in the data from the clinical study examined.

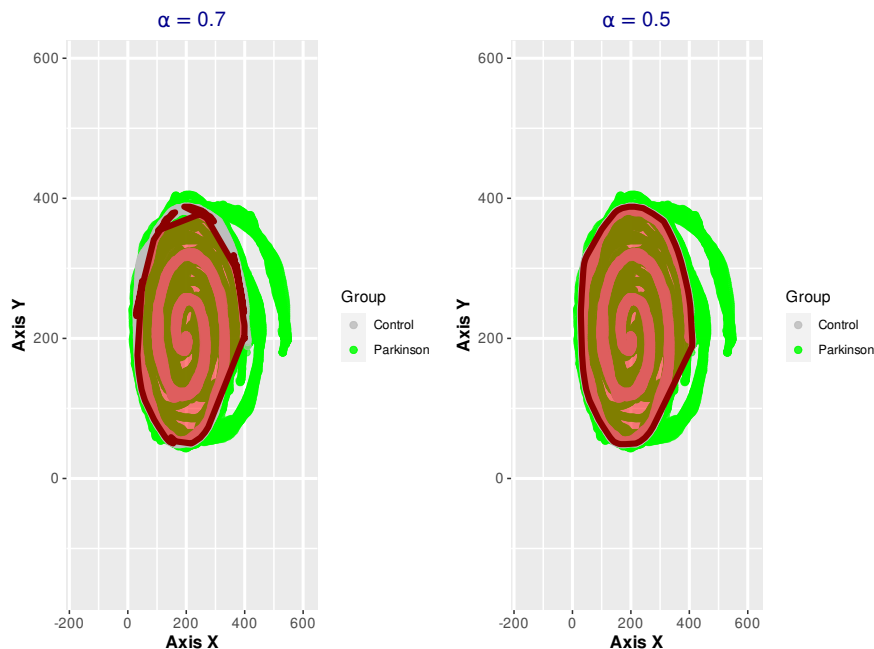


Figure 6: Tolerance regions in expectations for various confidence levels in the written test using control individuals as a reference. The plots depict the raw trajectories of both control and Parkinson’s patients. We do not introduce covariates in the derivation of prediction regions for the Fréchet mean.

## 4.2 Multidimensional Euclidean data

### 4.2.1 Motivation

Multivariate Euclidean data, denoted as  $\mathcal{Y} = \mathbb{R}^m$  ( $m > 1$ ), is increasingly prevalent in clinical outcome analysis, particularly in the integration of multiple biomarkers to enhance diagnostic accuracy for various diseases. This approach is exemplified in diabetes research, where at least two biomarkers – Fasting Plasma Glucose (FPG) and Glycosylated Hemoglobin (A1C) – are considered in the diagnosis of the disease. In this simple 2–dimensional example, providing naive uncertainty quantification measures is far from trivial due to the lack of a natural order in  $\mathbb{R}^2$ . Moreover, bivariate quantile estimation methods can depend on a specific notion of order tailored to each problem, as discussed in [Klein and Kneib, 2020]. This section aims to illustrate our uncertainty quantification framework, which can accommodate any distance  $d_2$  to define the prediction region  $C^\alpha(\cdot)$ , and overcome technical difficulties associated with defining a multivariate quantile. To emphasize the mathematical intuition behind our methods for defining prediction regions using balls, we consider the standard Euclidean distance  $d_2^2(x, y) = \sum_{i=1}^m (x_i - y_i)^2$  for all  $x, y \in \mathbb{R}^m$ . Continuing with the discussion on diabetes, we focus on a scientific application in this field. To demonstrate the application of our methodology, we consider the mentioned biomarkers: FPG and A1C as a response of the regression models that in this case will be a multivariate–response linear model.

The goal is to create a predictive models to estimate the continuous outcomed used to diagnostic and monitoring the progression of diabetes mellitus disease.

Uncertainty analysis is crucial in clinical prediction models, as it helps understand the advantages and disadvantages of these models. In cases where there is significant uncertainty in the regression model  $m$ , it may be necessary to construct a more complex model incorporating new patient characteristic attributes. Alternatively, considering more sophisticated regression models, such as neural networks, might enhance the predictive capacity of the models.

#### 4.2.2 Data Description

We conducted an extensive study using a comprehensive dataset from the National Health and Nutrition Examination Survey (NHANES) cohort (see more details [Matabuena et al., 2023a]), comprising a substantial number of individuals ( $n = 58,972$ ). For our analysis, we utilized predictor and response variables described in Table 2, and applied a linear multivariate regression model to estimate the function  $m$ . We considered  $k = 200$  as the number of neighbors in the kNN method.

Our study aimed to address two primary objectives: firstly, to demonstrate the remarkable computational efficiency of our algorithm, and secondly, to underscore the importance of quantifying uncertainty in standard disease risk scores. In an ideal clinical context, the primary clinical goal would be to establish a simple and cost-effective risk score that could accurately capture patients' glucose conditions without relying on traditional diabetes diagnostic variables, and stratify the risk of diabetes to promote new public health interventions [Matabuena et al., 2024b]. With uncertainty quantification, we can evaluate whether our regression model  $m$  can be useful for such clinical purposes.

#### 4.2.3 Results

The implementation of our algorithm in the NHANES dataset in the **R** software exhibited remarkable efficiency, with execution times of just a few seconds.

Figure 7 presents the results to apply the uncertainty quantification region in three patients. We observe individual uncertainty differences when we predict the A1C and FPG biomarkers based on individual clinical characteristics. Patient (C), characterized as young and healthy (see Table 2), is predicted to be in the non-diabetes range with low uncertainty. In contrast, patient (A), who is older, has a high waist circumference, and elevated systolic pressure, is predicted to fall within the diabetes and prediabetes range, despite exhibiting glucose profiles characteristic of a non-diabetic healthy individual. These outcomes underscore the need for more sophisticated variables to accurately predict the true glycemic patient status, as also evidenced by the marginal  $R^2$  for each variable that takes values equal to 0.12 and 0.08, respectively for the A1C and FPG.

In separate research [Matabuena et al., 2024b], we provide evidence that we need the incorporate at least one diabetes biomarker that directly measures the glucose of the individuals, such as FPG or A1C, is indispensable for building reliable predictive models. Essentially, this highlights that predicting Diabetes Mellitus is impossible without considering specific glucose measurements or proxy variables for them.

ID	Age	Waist	Systolic Pressure	Diastolic Pressure	Triglycerides	Glucose	Glycosylated Hemoglobin
45424 (A)	76	114.30	144	66	64	91.00	5.10
31858 (B)	55	107.70	128	70	72	98.00	7.60
28159 (C)	23	84.60	124	64	147	81.00	5.40

Table 2: Characteristics of three patients in a real-life example where the response variable is multivariate (bivariate) Euclidean data.

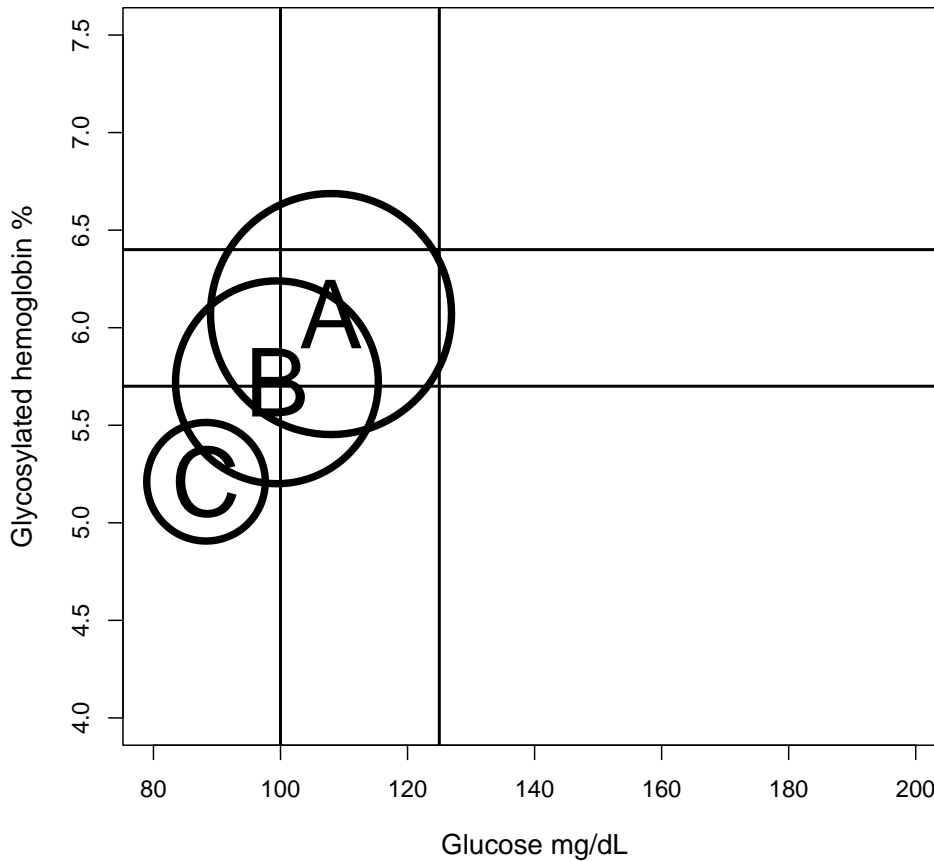


Figure 7: Prediction regions for three patients based on the geometry of the Euclidean distance. The black lines in the plot indicate the transition between prediabetes and diabetes status. Patient (C) is normoglycemic, while the other two patients, (A) and (B), exhibit oscillations between two glycemic statuses. Patient (B) is characterized as normoglycemic and diabetic, while patient A shows diabetes and prediabetes. The plot highlights the varying glycemic patterns according to patient characteristics.

### 4.3 Distributional Representation of Biosensor Time Series

#### 4.3.1 Motivation

The field of distributional data analysis has seen significant growth within data–science communities [Klein, 2023, Matabuena et al., 2022a, Meunier et al., 2022], largely due to its critical role in understanding the marginal distributional characteristics of biological time series in regression modeling. We investigate the probability distributions within continuous glucose monitor (CGM) time series data [Matabuena et al., 2021a], vital for discerning distributional patterns like hypoglycemia, and hyperglycemia in diabetes research. Figure 8 illustrates such mathematical transformation in the case of a one non-diabetic and diabetic individual

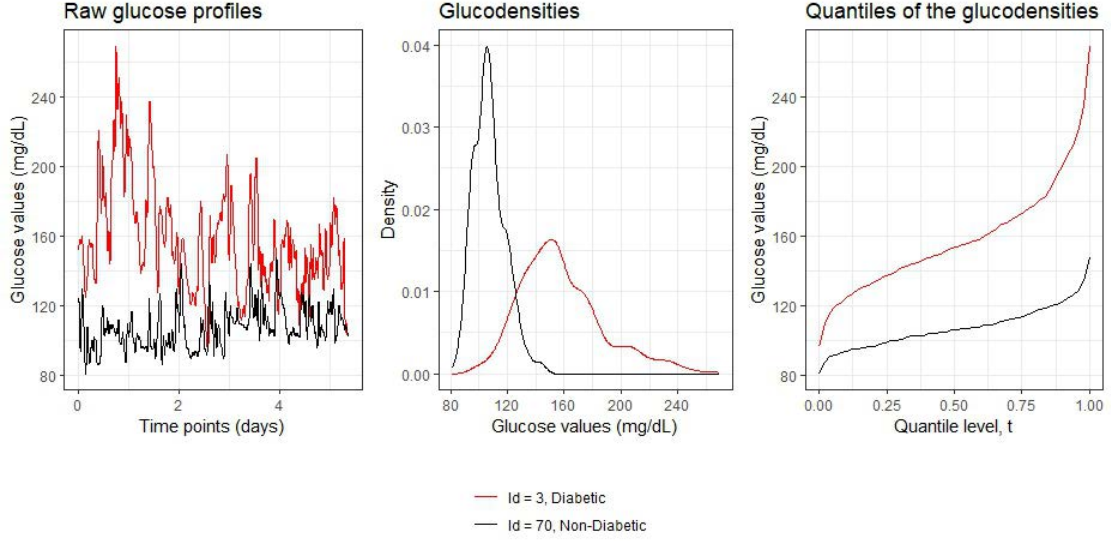


Figure 8: The figure presents the process of transformation CGM time series of two individuals in their marginal density functions and marginal quantile functions.

We focus on analyzing biological outcomes defined in the space  $\mathcal{Y} = \mathcal{W}_2(T)$ , comprising univariate continuous probability distributions on the compact support  $T = [40, 400] \subset \mathbb{R}$ . This work emphasizes "distributional representation" through quantile functions, aiming to enrich our understanding of glucose profiles' impacts from various factors beyond CGM simple summary as CGM mean and – standard deviation values estimated with the raw glucose time series.

Given a random sample of healthy individuals, the goal of our analysis is to provide the reference quantile glucose values with our uncertainty quantification algorithm across different age groups. The determination of this reference profile can have various applications, such as detecting individuals at high risk of diabetes mellitus, as well as determining threshold criteria considering the latest advancements about glucose homeostasis provided by a CGM monitor. We note that the glucose values at least, in average glucose levels increase with the age, and according to this biological behaviour, we must move to a medicine based on personalized criteria. The use of CGM one distributional representations allows to examine this biological phenomenon in all, low, middle and high-glucose concentrations.

### 4.3.2 Data Description

Data from [Shah et al., 2019], which collected glucose values at 5-minute intervals over several days from non-diabetic individuals in everyday settings, was considered in our analysis. This data was originally collected to establish normative glucose ranges with simple summaries as CGM mean values by age. Extending this foundation, we adopt the distributional perspective of CGM data as our regression model's response, utilizing the 2-Wasserstein distance (equivalently, quantile representation) in Global Fréchet regression. For analysis and visualization, we apply the supreme distance  $d_2(\cdot, \cdot) = \|\cdot - \cdot\|_\infty$ , setting the confidence level at  $\alpha = 0.2$  and the kNN smoothing parameter to  $k = 30$ .

### 4.3.3 Results

The application of our uncertainty quantification algorithm shows a variation in uncertainty levels across different age groups, as outlined in Figure 9. However, the analysis reveals a consistent conditional mean

of glucose across ages but a marked increase in the uncertainty of quantile glucose values with the increase of the age of patients. These clinical findings enhance our capability to classify and monitor health in non-diabetics through CGM. This approach to defining disease states offers a pathway towards personalized medicine, as evidenced by its application in our research on personalized sarcopenia definitions [Matabuena et al., 2023a], where the response variable was finite-dimensional outcome ( $\mathcal{Y} = \mathbb{R}^2$ ).

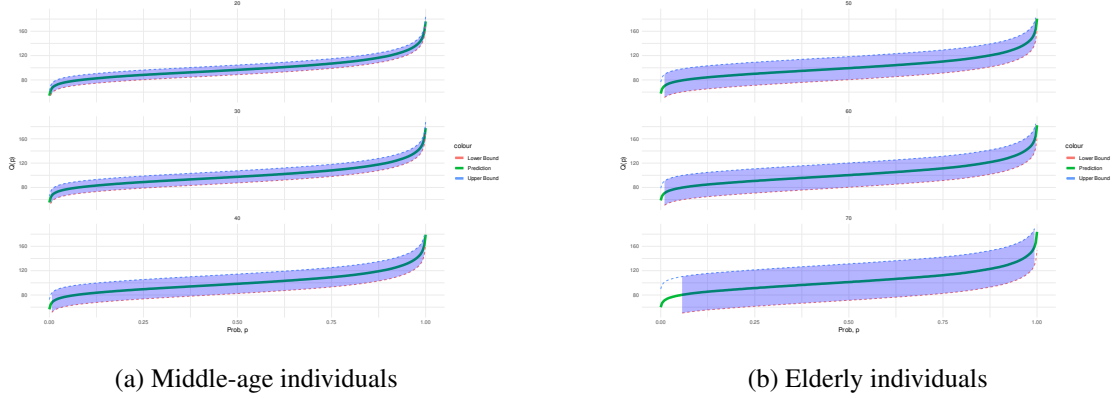


Figure 9: The figure presents the normative continuous glucose monitoring (CGM) distributional values across different age groups, with a confidence level  $\alpha = 0.2$ . Our analysis indicates that while the conditional mean values remain similar across different age groups, there is an increase in uncertainty as age increases.

## 4.4 Neuroimage Applications: Laplacian Graphs

### 4.4.1 Motivation

Neuroimaging represents important field that is motivated by the development of functional and metric space statistical methods in order to improve or understanding the behaviour of the human brain [Dubey and Müller, 2020, Dai et al., 2021, Bhattacharjee and Müller, 2022, Chen et al., 2021a]. Predominantly, functional magnetic resonance imaging (fMRI) serves as the benchmark for analyzing brain structures [Wang et al., 2021, Chen et al., 2021a, Pervaiz et al., 2020].

Summarizing fMRI data’s unique brain structure signatures involves generating individual profiles. These profiles estimate intra- and inter-regional cerebral connections through both continuous (correlation matrices) and discrete (graph structures) data representations [Wang et al., 2021].

There is a growing interest in applying uncertainty quantification techniques within neuroimaging. Yet, these methods predominantly employ univariate approaches, highlighting a need for more comprehensive models [Ernsting et al., 2023].

The goal of this analysis is to highlight the versatility of our algorithm to quantify the uncertainty over graphs. For each patient, a graph is available that measures the connectivity between different brain regions.

### 4.4.2 fMRI representation with Laplacian graphs

We begin by examining the continuous domain of Pearson correlation matrices  $\mathcal{Y}$  with dimension  $r$ , utilizing the Frobenius metric  $d_{\text{FRO}}(A, B) = \sqrt{\sum_{i,j=1}^r (A_{ij} - B_{ij})^2}$ . This approach extends to the network space, characterized by  $r$  nodes and employing the same metric for Laplacian matrices. To align graph spaces with their Laplacian representations, certain technical prerequisites are necessary.

Consider a network  $G_m = (V, E)$  with nodes  $V = \{v_1, \dots, v_r\}$  and edge weights  $E = \{w_{ij} : w_{ij} \geq 0; i, j = 1, \dots, r\}$ . We assume that  $G_m$  is a simple graph, devoid of self-loops or multiple edges and edge weights bounded  $0 \leq w_{ij} \leq w$ .

We define the graph Laplacian as the matrix  $L = (l_{ij})$ , where

$$l_{ij} = \begin{cases} -w_{ij}, & \text{if } i \neq j \\ \sum_{k \neq i} w_{ik}, & \text{if } i = j \end{cases}$$

for all indices  $i, j = 1, \dots, r$ . This definition leads to the characterization of the space of networks through the associated space of graph Laplacians, defined as:

$$\mathcal{L}_r = \{L = (l_{ij}) : L = L^T, L\mathbf{1}_r = \mathbf{0}_r, -W \leq l_{ij} \leq 0 \text{ for } i \neq j\},$$

where  $\mathbf{1}_r$  and  $\mathbf{0}_r$  denote the  $r$ -vectors of ones and zeroes, respectively.

#### 4.4.3 Data Description

Our study leverages an uncertainty quantification framework to analyze neuroimaging data, focusing on fMRI datasets from schizophrenia patients ( $n = 60$ ) and a control group ( $n = 45$ ) obtained from [Reli3n et al., 2019].

We utilized Laplacian graphs constructed from the data, following the preprocessing steps from [Reli3n et al., 2019]. In our analysis, we consider a unique predictor  $X \in \{0, 1\}$ , where  $X = 1$  indicates the schizophrenia of the individual.

#### 4.4.4 Results

Utilizing Global Fr3chet regression in the space of Laplacian networks  $\mathcal{Y} = (\mathcal{L}_r, d_{\text{FRO}})$ , which is equipped with the Frobenius distance applied to graph Laplacians, we estimated the regression function  $m$ . Subsequently, we applied the heteroscedastic uncertainty quantification algorithm with a fixed confidence level of  $\alpha = 0.2$  and a smoothing parameter  $k = 20$ . Figure 10 illustrates these conditional mean estimations along with their uncertainty intervals. The analysis reveals significant uncertainty, suggesting the potential utility of incorporating additional predictors to reduced the large uncertainty observed in the regression model.

### 4.5 Variable selection in physical activity example

Physical exercise is widely recognized as an effective non-pharmacological intervention for a broad range of diseases, as well as a means of mitigating physiological decline with age and improving overall health [Harridge and Lazarus, 2017]. Therefore, understanding the patient attributes that contribute to variations in physical activity levels is of great scientific interest and can inform the development of public health policies aimed at reducing disparities in physical activity across different subpopulations. In this study, we illustrate our variable selection methods for identifying relevant variables that are associated with physical activity levels of an individual.

#### 4.5.1 Data Description

This study used data from the combined 2011-2014 NHANES cohort, which involved a comprehensive array of standardized health examinations and medical tests. These evaluations covered biochemical, dietary, physical activity, and anthropometric assessments. To measure physical activity levels at high resolution, the study utilized the ActiGraph GT3X+ accelerometer (Actigraph, Pensacola, FL) worn on the

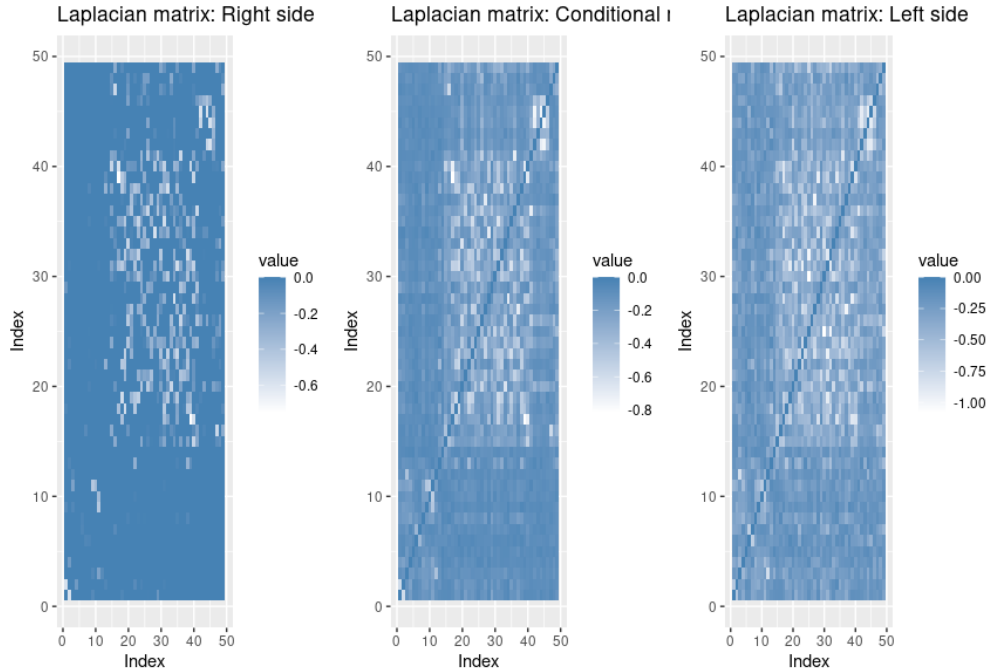


Figure 10: Left: Conditional mean function. Center: Left end of the uncertainty set. Right: Right end of the uncertainty set. Uncertainty analysis from a patient with schizophrenia using as a confidence level 20 percent.

non-dominant wrist for seven full and two partial days among a subsample of participants. Further details regarding the specific protocols for collecting NHANES variables can be accessed on the official website at <https://www.cdc.gov/nchs/nhanes/index.htm>.

In our investigation, we adopt a functional perspective to summarize physical activity profiles using distributional quantile representations. These representations are equipped with the 2 Wasserstein distance ( $\mathcal{W} = \mathcal{W}_2([a, b])$ ), as originally proposed in [Matabuena and Petersen, 2023]. Our predictor variables include gender, age, waist circumference, glucose levels, and a scalar summary of energetic expenditure, total activity count, and diet health score. We posited that the biochemical variable glucose would exhibit a weak association with physical activity levels, while the summary physical activity variables and diet would display a stronger relationship. Moreover, we anticipated that the remaining variables would demonstrate moderate connections with daily physical activity and energy expenditure.

#### 4.5.2 Results

The global importance of relevant and non-relevant variables for predicting distributional physical activity representations is summarized in Table 3. Initially, based on our hypothesis, we expected glucose to be non-relevant, while waist circumference would exhibit a statistical association with the response. However, the results of the new variable selection method surprised us, indicating that waist circumference is not a significant variable. This unexpected outcome can be attributed to the fact that the effect of waist is already captured directly by the total activity count (TAC), as both variables are correlated.

To visually illustrate the local importance of the analyzed variables, we present Figure 2. The figure depicts the intensity of importance for each value of the predictor on the y-axis. Notably, in our application, the

importance of the variables increases with higher values. This trend is particularly pronounced for the TAC variable, where larger TAC values correspond to higher variable importance.

Both Table 3 and Figure 2 offer valuable insights into the relevance and importance of the variables in predicting distributional physical activity representations. These findings contribute to understanding the individual characteristics that impact physical activity profiles.

Variable No.	Variable Name	Selected	Raw p-value
1	<b>Gender</b>	TRUE	0.003
2	<b>Age</b>	TRUE	< 0.001
3	<b>Waist</b>	FALSE	< 0.26
4	<b>TAC</b>	TRUE	< 0.001
5	<b>Healthy Eating Index</b>	TRUE	< 0.001
6	<b>Glucose Values</b>	FALSE	< 0.04

Table 3: Summary of results from applying a new variable selection method to predict distributional physical activity representations using data from the NHANES 2011-2014 dataset. Variable No. indicates the variable number in the Figure 2.

## 5 Discussion

This paper introduces a novel data analysis framework designed to quantify uncertainty in regression models with random responses taking values in metric spaces. Our approach demonstrates versatility, applicable to a wide range of regression algorithms, and operates under minimal theoretical conditions. Our method provides non-asymptotic guarantees in homoscedastic cases. Furthermore, this novel uncertainty quantification framework extends the notion of conditional quantile function for metric space responses [Liu et al., 2022].

In the context of homoscedasticity, our approach represents a natural generalization of split conformal methods by incorporating the distance function  $d_2$  as a conformity score. For the heteroscedastic case, we draw upon recent work by Györfi and Walk on univariate responses [Györfi and Walk, 2019], extending their methodology to metric spaces. Through extensive simulations and theoretical analysis, we validate the effectiveness of our method and highlight its properties in various settings.

We acknowledge that in the heteroscedastic case, the selection of model hyperparameters, specifically  $d_2$ , and  $k$ , smoothing parameter, can significantly impact the quality of final estimator results. To address this issue effectively, we propose exploring stability selection techniques [Meinshausen and Bühlmann, 2010] and other resampling techniques based on bootstrap for the kNN method, as proposed in the literature [Hall et al., 2008, Samworth, 2012]. Investigating these approaches in future research is anticipated to offer valuable solutions to the tuning parameter problem.

The effectiveness of our approach is demonstrated through different relevant medical examples. For example, we present a novel application in diabetes, proposing normative distributional glucose values across different age groups using the notion of glucodensity [Matabuena et al., 2021a]. Currently, the use of CGM devices in diabetes research is of increasing interest [Keshet et al., 2023], and our applications have contributed to this direction in human health research.

Moreover, we have developed a variable selection method for metric space responses. This method is computationally efficient. Importantly, our approach integrates into other semiparametric models, such as the partial single index Fréchet model [Ghosal et al., 2023], distinguishing it from existing variable selection methods in metric spaces that are limited to the global Fréchet regression model [Tucker et al., 2021].

Future research directions for our method are geared towards expanding its applicability and advancing its capabilities in handling diverse data scenarios and structures. One crucial aspect is extending the uncertainty

quantification framework to effectively handle temporally and spatially correlated data, enabling us to tackle more complex real-world situations. Additional relevant direction could include the accommodation of non-Euclidean predictors [Cohen and Kontorovich, 2022].

## Acknowledgments

This research was partially supported by US Horizon 2020 research and innovation program under grant agreement No. 952215 (TAILOR Connectivity Fund). Gábor Lugosi acknowledges the support of Ayudas Fundación BBVA a Proyectos de Investigación Científica 2021 and the Spanish Ministry of Economy and Competitiveness, Grant PGC2018-101643-B-I00 and FEDER, EU.

## References

- [Angelopoulos and Bates, 2023] Angelopoulos, A. N. and Bates, S. (2023). Conformal prediction: A gentle introduction. *Foundations and Trends® in Machine Learning*, 16(4):494–591.
- [Banerji et al., 2023] Banerji, C. R. S., Chakraborti, T., Harbron, C., and MacArthur, B. D. (2023). Clinical ai tools must convey predictive uncertainty for each individual patient. *Nature Medicine*.
- [Barber et al., 2023] Barber, R. F., Candès, E. J., Ramdas, A., and Tibshirani, R. J. (2023). Conformal prediction beyond exchangeability. *The Annals of Statistics*, 51(2):816 – 845.
- [Bates et al., 2023] Bates, S., Candès, E., Lei, L., Romano, Y., and Sesia, M. (2023). Testing for outliers with conformal p-values. *The Annals of Statistics*, 51(1):149–178.
- [Bhattacharjee et al., 2023] Bhattacharjee, S., Li, B., and Xue, L. (2023). Nonlinear global fréchet regression for random objects via weak conditional expectation. *arXiv preprint arXiv:2310.07817*.
- [Bhattacharjee and Müller, 2021] Bhattacharjee, S. and Müller, H.-G. (2021). Single index fréchet regression. *arXiv preprint arXiv:2108.05437*.
- [Bhattacharjee and Müller, 2022] Bhattacharjee, S. and Müller, H.-G. (2022). Concurrent object regression. *Electronic Journal of Statistics*, 16(2):4031–4089.
- [Bhattacharjee and Müller, 2023] Bhattacharjee, S. and Müller, H.-G. (2023). Geodesic mixed effects models for repeatedly observed/longitudinal random objects. *arXiv preprint arXiv:2307.05726*.
- [Biau and Devroye, 2015] Biau, G. and Devroye, L. (2015). *Lectures on the nearest neighbor method*, volume 246. Springer.
- [Boehm Vock et al., 2015] Boehm Vock, L. F., Reich, B. J., Fuentes, M., and Dominici, F. (2015). Spatial variable selection methods for investigating acute health effects of fine particulate matter components. *Biometrics*, 71(1):167–177.
- [Bulté and Sørensen, 2023] Bulté, M. and Sørensen, H. (2023). Medoid splits for efficient random forests in metric spaces. *arXiv preprint arXiv:2306.17031*.
- [Candès et al., 2023] Candès, E., Lei, L., and Ren, Z. (2023). Conformalized survival analysis. *Journal of the Royal Statistical Society Series B: Statistical Methodology*, 85(1):24–45.
- [Cauchois et al., 2021] Cauchois, M., Gupta, S., and Duchi, J. C. (2021). Knowing what you know: valid and validated confidence sets in multiclass and multilabel prediction. *Journal of Machine Learning Research*, 22(81):1–42.

- [Chen and Müller, 2023] Chen, H. and Müller, H.-G. (2023). Sliced wasserstein regression. *arXiv preprint arXiv:2306.10601*.
- [Chen et al., 2021a] Chen, Y., Dubey, P., Müller, H.-G., Bruchhage, M., Wang, J.-L., and Deoni, S. (2021a). Modeling sparse longitudinal data in early neurodevelopment. *NeuroImage*, 237:118079.
- [Chen et al., 2021b] Chen, Y., Lin, Z., and Müller, H.-G. (2021b). Wasserstein regression. *Journal of the American Statistical Association*, 116(535):1–14.
- [Cheng and Yang, 2022] Cheng, J. and Yang, P. (2022). Conformal inference for heterogeneous policy effect.
- [Chernozhukov et al., 2021a] Chernozhukov, V., Wüthrich, K., and Zhu, Y. (2021a). Distributional conformal prediction. *Proceedings of the National Academy of Sciences*, 118(48):e2107794118.
- [Chernozhukov et al., 2021b] Chernozhukov, V., Wüthrich, K., and Zhu, Y. (2021b). An exact and robust conformal inference method for counterfactual and synthetic controls. *Journal of the American Statistical Association*, 116(536):1849–1864.
- [Chhikara and Guttman, 1982] Chhikara, R. S. and Guttman, I. (1982). Prediction limits for the inverse gaussian distribution. *Technometrics*, 24(4):319–324.
- [Cohen and Kontorovich, 2022] Cohen, D. T. and Kontorovich, A. (2022). Metric-valued regression. *ArXiv Preprint*.
- [Cover, 1968] Cover, T. (1968). Estimation by the nearest neighbor rule. *IEEE Transactions on Information Theory*, 14(1):50–55.
- [Dai et al., 2021] Dai, X., Lin, Z., and Müller, H.-G. (2021). Modeling sparse longitudinal data on Riemannian manifolds. *Biometrics*, 77(4):1328–1341.
- [Das et al., 2022] Das, S., Zhang, Y., and Politis, D. N. (2022). Model-based and model-free point prediction algorithms for locally stationary random fields. *arXiv preprint arXiv:2212.03079*.
- [Devroye, 1981] Devroye, L. (1981). On the Almost Everywhere Convergence of Nonparametric Regression Function Estimates. *The Annals of Statistics*, 9(6):1310 – 1319.
- [Dietterich and Hostetler, ] Dietterich, T. and Hostetler, J. Reinforcement learning prediction intervals with guaranteed fidelity.
- [Dietterich and Hostetler, 2022] Dietterich, T. G. and Hostetler, J. (2022). Conformal prediction intervals for markov decision process trajectories. *arXiv preprint arXiv:2206.04860*.
- [Diquigiovanni et al., 2022] Diquigiovanni, J., Fontana, M., and Vantini, S. (2022). Conformal prediction bands for multivariate functional data. *Journal of Multivariate Analysis*, 189:104879.
- [Dryden and Mardia, 2016] Dryden, I. L. and Mardia, K. V. (2016). *Statistical shape analysis: with applications in R*, volume 995. John Wiley & Sons.
- [Dubey et al., 2022] Dubey, P., Chen, Y., and Müller, H.-G. (2022). Depth profiles and the geometric exploration of random objects through optimal transport. *arXiv preprint arXiv:2202.06117*.
- [Dubey and Müller, 2019] Dubey, P. and Müller, H.-G. (2019). Fréchet analysis of variance for random objects. *Biometrika*, 106(4):803–821.

- [Dubey and Müller, 2020] Dubey, P. and Müller, H.-G. (2020). Functional models for time-varying random objects. *Journal of the Royal Statistical Society: Series B (Statistical Methodology)*, 82(2):275–327.
- [Dubey and Müller, 2022] Dubey, P. and Müller, H.-G. (2022). Modeling time-varying random objects and dynamic networks. *Journal of the American Statistical Association*, 117(540):2252–2267.
- [Dunn et al., 2022] Dunn, R., Wasserman, L., and Ramdas, A. (2022). Distribution-free prediction sets for two-layer hierarchical models. *Journal of the American Statistical Association*, pages 1–12.
- [Ernsting et al., 2023] Ernsting, J., Winter, N. R., Leenings, R., Sarink, K., Barkhau, C. B. C., Fisch, L., Emden, D., Holstein, V., Repple, J., Grotegerd, D., Meinert, S., Investigators, N., Berger, K., Risse, B., Dannlowski, U., and Hahn, T. (2023). From group-differences to single-subject probability: Conformal prediction-based uncertainty estimation for brain-age modeling.
- [Fan and Müller, 2021] Fan, J. and Müller, H.-G. (2021). Conditional Wasserstein barycenters and interpolation/extrapolation of distributions. *arXiv preprint arXiv:2107.09218*.
- [Fix and Hodges, 1951] Fix, E. and Hodges, J. (1951). Discriminatory analysis, nonparametric discrimination usa school of medicine. *Texas: Rendolph Field*, 1952.
- [Fong and Holmes, 2021] Fong, E. and Holmes, C. C. (2021). Conformal bayesian computation. *Advances in Neural Information Processing Systems*, 34:18268–18279.
- [Fontana et al., 2023] Fontana, M., Zeni, G., and Vantini, S. (2023). Conformal prediction: a unified review of theory and new challenges. *Bernoulli*, 29(1):1–23.
- [Fout and Fosdick, 2023] Fout, A. and Fosdick, B. K. (2023). Fréchet covariance and manova tests for random objects in multiple metric spaces. *arXiv preprint arXiv:2306.12066*.
- [Foygel Barber et al., 2021] Foygel Barber, R., Candès, E. J., Ramdas, A., and Tibshirani, R. J. (2021). The limits of distribution-free conditional predictive inference. *Information and Inference: A Journal of the IMA*, 10(2):455–482.
- [Fraser and Guttman, 1956] Fraser, D. A. and Guttman, I. (1956). Tolerance regions. *The Annals of Mathematical Statistics*, 27(1):162–179.
- [Fréchet, 1948] Fréchet, M. R. (1948). Les éléments aléatoires de nature quelconque dans un espace distancié. *Annales de l’institut Henri Poincaré*, 10(4):215–310.
- [Gammerman et al., 1998] Gammerman, A., Vladimir, V., and Vapnik, V. (1998). Learning by transduction. In *Proceedings of the 1st Annual Conference on Uncertainty in Artificial Intelligence (UAI-85)*, pages 148–155.
- [García-Meixide and Matabuena, 2023] García-Meixide, C. and Matabuena, M. (2023). Causal survival embeddings: non-parametric counterfactual inference under censoring. *arXiv preprint arXiv:2306.11704*.
- [Gawlikowski et al., 2023] Gawlikowski, J., Tassi, C. R. N., Ali, M., Lee, J., Humt, M., Feng, J., Kruspe, A., Triebel, R., Jung, P., Roscher, R., et al. (2023). A survey of uncertainty in deep neural networks. *Artificial Intelligence Review*, pages 1–77.
- [Geenens et al., 2023] Geenens, G., Nieto-Reyes, A., and Francisci, G. (2023). Statistical depth in abstract metric spaces. *Statistics and Computing*, 33(2):46.

- [Geisser, 2017] Geisser, S. (2017). *Predictive inference*. Chapman and Hall/CRC.
- [Ghosal et al., 2023] Ghosal, A., Matabuena, M., Meiring, W., and Petersen, A. (2023). Predicting distributional profiles of physical activity in the nhanes database using a partially linear single-index fréchet regression model. *arXiv preprint arXiv:2302.07692*.
- [Ghosal and Matabuena, 2023] Ghosal, R. and Matabuena, M. (2023). Multivariate scalar on multidimensional distribution regression.
- [Ghosal et al., 2021a] Ghosal, R., Varma, V. R., Volfson, D., Hillel, I., Urbanek, J., Hausdorff, J. M., Watts, A., and Zipunnikov, V. (2021a). Distributional data analysis via quantile functions and its application to modelling digital biomarkers of gait in Alzheimer’s disease. *Biostatistics*. kxab041.
- [Ghosal et al., 2021b] Ghosal, R., Varma, V. R., Volfson, D., Urbanek, J., Hausdorff, J. M., Watts, A., and Zipunnikov, V. (2021b). Scalar on time-by-distribution regression and its application for modelling associations between daily-living physical activity and cognitive functions in alzheimer’s disease. *arXiv preprint arXiv:2106.03979*.
- [Gibbs et al., 2023] Gibbs, I., Cherian, J. J., and Candès, E. J. (2023). Conformal prediction with conditional guarantees. *arXiv preprint arXiv:2305.12616*.
- [Goldfeld and Quandt, 1965] Goldfeld, S. M. and Quandt, R. E. (1965). Some tests for homoscedasticity. *Journal of the American statistical Association*, 60(310):539–547.
- [Györfi and Walk, 2019] Györfi, L. and Walk, H. (2019). Nearest neighbor based conformal prediction. In *Annales de l’ISUP*, volume 63, pages 173–190.
- [Hall et al., 2008] Hall, P., Park, B. U., and Samworth, R. J. (2008). Choice of neighbor order in nearest-neighbor classification.
- [Hamada et al., 2004] Hamada, M., Johnson, V., Moore, L. M., and Wendelberger, J. (2004). Bayesian prediction intervals and their relationship to tolerance intervals. *Technometrics*, 46(4):452–459.
- [Hammouri et al., 2023] Hammouri, Z. A. A., Mier, P. R., Félix, P., Mansournia, M. A., Huelin, F., Casals, M., and Matabuena, M. (2023). Uncertainty quantification in medicine science: The next big step. *Archivos de Bronconeumología*.
- [Hanneke, 2022] Hanneke, S. (2022). Universally consistent online learning with arbitrarily dependent responses. In *International Conference on Algorithmic Learning Theory*, pages 488–497. PMLR.
- [Harridge and Lazarus, 2017] Harridge, S. D. and Lazarus, N. R. (2017). Physical activity, aging, and physiological function. *Physiology*, 32(2):152–161.
- [Harville, 1976] Harville, D. (1976). Extension of the gauss-markov theorem to include the estimation of random effects. *The Annals of Statistics*, 4(2):384–395.
- [Hu and Lei, 2023] Hu, X. and Lei, J. (2023). A two-sample conditional distribution test using conformal prediction and weighted rank sum. *Journal of the American Statistical Association*, pages 1–19.
- [Isenkul et al., 2014] Isenkul, M., Sakar, B., Kursun, O., et al. (2014). Improved spiral test using digitized graphics tablet for monitoring parkinson’s disease. In *The 2nd international conference on e-health and telemedicine (ICEHTM-2014)*, volume 5, pages 171–175.
- [Jeon et al., 2022] Jeon, J. M., Lee, Y. K., Mammen, E., and Park, B. U. (2022). Locally polynomial Hilbertian additive regression. *Bernoulli*, 28(3):2034 – 2066.

- [Jin et al., 2023] Jin, Y., Ren, Z., and Candès, E. J. (2023). Sensitivity analysis of individual treatment effects: A robust conformal inference approach. *Proceedings of the National Academy of Sciences*, 120(6):e2214889120.
- [Johnstone and Cox, 2021] Johnstone, C. and Cox, B. (2021). Conformal uncertainty sets for robust optimization. In *Conformal and Probabilistic Prediction and Applications*, pages 72–90. PMLR.
- [Johnstone and Ndiaye, 2022] Johnstone, C. and Ndiaye, E. (2022). Exact and approximate conformal inference in multiple dimensions. *arXiv preprint arXiv:2210.17405*.
- [Keshet et al., 2023] Keshet, A., Shilo, S., Godneva, A., Talmor-Barkan, Y., Aviv, Y., Segal, E., and Rossman, H. (2023). Cgmap: Characterizing continuous glucose monitor data in thousands of non-diabetic individuals. *Cell Metabolism*, 35(5):758–769.e3.
- [Klein, 2023] Klein, N. (2023). Distributional regression for data analysis. *arXiv preprint arXiv:2307.10651*.
- [Klein and Kneib, 2020] Klein, N. and Kneib, T. (2020). Directional bivariate quantiles: a robust approach based on the cumulative distribution function. *AStA Advances in Statistical Analysis*, 104(2):225–260.
- [Kneib et al., 2021] Kneib, T., Silbersdorff, A., and Säfken, B. (2021). Rage against the mean—a review of distributional regression approaches. *Econometrics and Statistics*.
- [Kuchibhotla, 2020] Kuchibhotla, A. K. (2020). Exchangeability, conformal prediction, and rank tests. *arXiv preprint arXiv:2005.06095*.
- [Kurusu and Otsu, ] Kurisu, D. and Otsu, T. Model averaging for global fréchet regression.
- [Lei et al., 2018] Lei, J., G’Sell, M., Rinaldo, A., Tibshirani, R. J., and Wasserman, L. (2018). Distribution-free predictive inference for regression. *Journal of the American Statistical Association*, 113(523):1094–1111.
- [Lei et al., 2013] Lei, J., Robins, J., and Wasserman, L. (2013). Distribution-free prediction sets. *Journal of the American Statistical Association*, 108(501):278–287.
- [Lei and Wasserman, 2014] Lei, J. and Wasserman, L. (2014). Distribution-free prediction bands for non-parametric regression. *Journal of the Royal Statistical Society: Series B: Statistical Methodology*, pages 71–96.
- [Li and Liu, 2008] Li, J. and Liu, R. Y. (2008). Multivariate spacings based on data depth: I. construction of nonparametric multivariate tolerance regions. *The Annals of Statistics*, 36(3):1299–1323.
- [Li et al., 2022] Li, X., Ghosh, J., and Villarini, G. (2022). A comparison of bayesian multivariate versus univariate normal regression models for prediction. *The American Statistician*, 0(0):1–9.
- [Lin et al., 2023] Lin, Z., Müller, H.-G., and Park, B. (2023). Additive models for symmetric positive-definite matrices and lie groups. *Biometrika*, 110(2):361–379.
- [Liu et al., 2022] Liu, H., Wang, X., and Zhu, J. (2022). Quantiles, ranks and signs in metric spaces. *arXiv preprint arXiv:2209.04090*.
- [Lu et al., 2023] Lu, C., Yu, Y., Karimireddy, S. P., Jordan, M., and Raskar, R. (2023). Federated conformal predictors for distributed uncertainty quantification. In *International Conference on Machine Learning*, pages 22942–22964. PMLR.

- [Lu, 2023] Lu, H. (2023). *Data Augmentation and Conformal Prediction*. PhD thesis, Massachusetts Institute of Technology.
- [Lyons, 2013] Lyons, R. (2013). Distance covariance in metric spaces. *The Annals of Probability*, 41(5):3284–3305.
- [Lyons, 2021] Lyons, R. (2021). Second errata to distance covariance in metric spaces. *The Annals of Probability*, 49(5):2668 – 2670.
- [Major, 1978] Major, P. (1978). On the invariance principle for sums of independent identically distributed random variables. *Journal of Multivariate Analysis*, 8(4):487–517.
- [Matabuena, 2022] Matabuena, M. (2022). *Contributions on metric spaces with applications in personalized medicine*. PhD thesis, Universidade de Santiago de Compostela.
- [Matabuena et al., 2023a] Matabuena, M., Abdalla, P. P., Machado, D. R. L., Bohn, L., and Mota, J. (2023a). Handgrip strength conditional tolerance regions suggest the need for personalized sarcopenia definition: an analysis of the american nhanes database. *Aging Clinical and Experimental Research*, 35(6):1369–1373.
- [Matabuena and Crainiceanu, 2024] Matabuena, M. and Crainiceanu, C. M. (2024). Multilevel functional distributional models with application to continuous glucose monitoring in diabetes clinical trials. *arXiv preprint arXiv:2403.10514*.
- [Matabuena et al., 2024a] Matabuena, M., Díaz-Louzao, C., Ghosal, R., and Gude, F. (2024a). Personalized imputation in metric spaces via conformal prediction: Applications in predicting diabetes development with continuous glucose monitoring information.
- [Matabuena et al., 2023b] Matabuena, M., Félix, P., Ditzhaus, M., Vidal, J., and Gude, F. (2023b). Hypothesis testing for matched pairs with missing data by maximum mean discrepancy: An application to continuous glucose monitoring. *The American Statistician*, 0(0):1–13.
- [Matabuena et al., 2022a] Matabuena, M., Félix, P., García-Meixide, C., and Gude, F. (2022a). Kernel machine learning methods to handle missing responses with complex predictors. application in modelling five-year glucose changes using distributional representations. *Computer Methods and Programs in Biomedicine*, page 106905.
- [Matabuena et al., 2022b] Matabuena, M., Félix, P., Hammouri, Z. A. A., Mota, J., and del Pozo Cruz, B. (2022b). Physical activity phenotypes and mortality in older adults: a novel distributional data analysis of accelerometry in the nhanes. *Aging Clinical and Experimental Research*, pages 1–8.
- [Matabuena and Petersen, 2023] Matabuena, M. and Petersen, A. (2023). Distributional data analysis of accelerometer data from the NHANES database using nonparametric survey regression models. *Journal of the Royal Statistical Society Series C: Applied Statistics*, 72(2):294–313.
- [Matabuena et al., 2021a] Matabuena, M., Petersen, A., Vidal, J. C., and Gude, F. (2021a). Glucodensities: A new representation of glucose profiles using distributional data analysis. *Statistical Methods in Medical Research*, 30(6):1445–1464. PMID: 33760665.
- [Matabuena et al., 2021b] Matabuena, M., Rodríguez-Mier, P., García-Meixide, C., and Leborán, V. (2021b). Covid-19: Estimation of the transmission dynamics in spain using a stochastic simulator and black-box optimization techniques. *Computer methods and programs in biomedicine*, 211:106399.

- [Matabuena et al., 2024b] Matabuena, M., Vidal, J. C., Ghosal, R., and Onnela, J.-P. (2024b). Deep learning framework with uncertainty quantification for survey data: Assessing and predicting diabetes mellitus risk in the american population.
- [Meinshausen and Bühlmann, 2010] Meinshausen, N. and Bühlmann, P. (2010). Stability selection. *Journal of the Royal Statistical Society: Series B (Statistical Methodology)*, 72(4):417–473.
- [Messoudi et al., 2022] Messoudi, S., Destercke, S., and Rousseau, S. (2022). Ellipsoidal conformal inference for multi-target regression. In *Conformal and Probabilistic Prediction with Applications*, pages 294–306. PMLR.
- [Meunier et al., 2022] Meunier, D., Pontil, M., and Ciliberto, C. (2022). Distribution regression with sliced Wasserstein kernels. In Chaudhuri, K., Jegelka, S., Song, L., Szepesvari, C., Niu, G., and Sabato, S., editors, *Proceedings of the 39th International Conference on Machine Learning*, volume 162 of *Proceedings of Machine Learning Research*, pages 15501–15523. PMLR.
- [Panaretos and Zemel, 2020] Panaretos, V. M. and Zemel, Y. (2020). *An invitation to statistics in Wasserstein space*. Springer Nature.
- [Patel et al., 2023] Patel, Y., McNamara, D., Loper, J., Regier, J., and Tewari, A. (2023). Variational inference with coverage guarantees. *arXiv preprint arXiv:2305.14275*.
- [Pervaiz et al., 2020] Pervaiz, U., Vidaurre, D., Woolrich, M. W., and Smith, S. M. (2020). Optimising network modelling methods for fMRI. *Neuroimage*, 211:116604.
- [Petersen et al., 2021] Petersen, A., Liu, X., and Divani, A. A. (2021). Wasserstein  $F$ -tests and confidence bands for the Fréchet regression of density response curves. *The Annals of Statistics*, 49(1):590 – 611.
- [Petersen and Müller, 2019] Petersen, A. and Müller, H.-G. (2019). Fréchet regression for random objects with euclidean predictors. *The Annals of Statistics*, 47(2):691–719.
- [Politis, 2015] Politis, D. N. (2015). Model-free prediction in regression. In *Model-Free Prediction and Regression*, pages 57–80. Springer.
- [Politis and Romano, 1994] Politis, D. N. and Romano, J. P. (1994). Large sample confidence regions based on subsamples under minimal assumptions. *The Annals of Statistics*, pages 2031–2050.
- [Qiu et al., 2024] Qiu, R., Yu, Z., and Lin, Z. (2024). Semi-supervised fréchet regression.
- [Relión et al., 2019] Relión, J. D. A., Kessler, D., Levina, E., and Taylor, S. F. (2019). Network classification with applications to brain connectomics. *The Annals of Applied Statistics*, 13(3):1648–1667.
- [Romano et al., 2019] Romano, Y., Patterson, E., and Candès, E. (2019). Conformalized quantile regression. *Advances in Neural Information Processing Systems*, 32:3543–3553.
- [Samworth, 2012] Samworth, R. J. (2012). Optimal weighted nearest neighbour classifiers.
- [Schötz, 2021] Schötz, C. (2021). *The Fréchet Mean and Statistics in Non-Euclidean Spaces*. PhD thesis.
- [Seber and Lee, 2003] Seber, G. A. and Lee, A. J. (2003). *Linear regression analysis*, volume 330. John Wiley & Sons.
- [Sesia and Candès, 2020] Sesia, M. and Candès, E. J. (2020). A comparison of some conformal quantile regression methods. *Stat*, 9(1):e261. e261 sta4.261.

- [Shafer and Vovk, 2008] Shafer, G. and Vovk, V. (2008). A tutorial on conformal prediction. *Journal of Machine Learning Research*, 9(3).
- [Shah et al., 2019] Shah, V. N., DuBose, S. N., Li, Z., Beck, R. W., Peters, A. L., Weinstock, R. S., Kruger, D., Tansey, M., Sparling, D., Woerner, S., et al. (2019). Continuous glucose monitoring profiles in healthy nondiabetic participants: a multicenter prospective study. *The Journal of Clinical Endocrinology & Metabolism*, 104(10):4356–4364.
- [Shapiro et al., 2023] Shapiro, I., Stein, J., MacRae, C., and O’Reilly, M. (2023). Pulse oximetry values from 33,080 participants in the apple heart & movement study. *npj Digital Medicine*, 6(1):134.
- [Singh et al., 2023] Singh, S., Sarna, N., Re, M., Li, Y., Lin, Y., Orfanoudaki, A., and Berger, M. (2023). Distribution-free risk assessment of regression-based machine learning algorithms. *arXiv preprint arXiv:2310.03545*.
- [Solari and Djordjilović, 2022] Solari, A. and Djordjilović, V. (2022). Multi split conformal prediction. *Statistics & Probability Letters*, 184:109395.
- [Steyer et al., 2023] Steyer, L., Stöcker, A., and Greven, S. (2023). Elastic analysis of irregularly or sparsely sampled curves. *Biometrics*, 79(3):2103–2115.
- [Sun, 2022] Sun, S. (2022). Conformal methods for quantifying uncertainty in spatiotemporal data: A survey. *arXiv preprint arXiv:2209.03580*.
- [Székely and Rizzo, 2017] Székely, G. J. and Rizzo, M. L. (2017). The energy of data. *Annual Review of Statistics and Its Application*, 4:447–479.
- [Székely et al., 2007a] Székely, G. J., Rizzo, M. L., and Bakirov, N. K. (2007a). Measuring and testing dependence by correlation of distances. *The Annals of Statistics*, 35(6):2769 – 2794.
- [Székely et al., 2007b] Székely, G. J., Rizzo, M. L., and Bakirov, N. K. (2007b). Measuring and testing dependence by correlation of distances. *The Annals of Statistics*, 35(6):2769–2794.
- [Teng et al., 2021] Teng, J., Tan, Z., and Yuan, Y. (2021). T-sci: A two-stage conformal inference algorithm with guaranteed coverage for cox-mlp. In *International Conference on Machine Learning*, pages 10203–10213. PMLR.
- [Thombs and Schucany, 1990] Thombs, L. A. and Schucany, W. R. (1990). Bootstrap prediction intervals for autoregression. *Journal of the American Statistical Association*, 85(410):486–492.
- [Tu et al., 2020] Tu, J., Torrente-Rodríguez, R. M., Wang, M., and Gao, W. (2020). The era of digital health: A review of portable and wearable affinity biosensors. *Advanced Functional Materials*, 30(29):1906713.
- [Tucker et al., 2021] Tucker, D. C., Wu, Y., and Müller, H.-G. (2021). Variable selection for global fréchet regression. *Journal of the American Statistical Association*, 0(0):1–15.
- [Virta, 2023] Virta, J. (2023). Spatial depth for data in metric spaces. *arXiv preprint arXiv:2306.09740*.
- [Vovk, 2012] Vovk, V. (2012). Conditional validity of inductive conformal predictors. In *Asian conference on machine learning*, pages 475–490. PMLR.
- [Vovk et al., 2005] Vovk, V., Gammerman, A., and Shafer, G. (2005). *Algorithmic learning in a random world*, volume 29. Springer.

- [Vovk et al., 2018] Vovk, V., Nouretdinov, I., Manokhin, V., and Gammerman, A. (2018). Cross-conformal predictive distributions. In *Conformal and Probabilistic Prediction and Applications*, pages 37–51. PMLR.
- [Wang and Leng, 2008] Wang, H. and Leng, C. (2008). A note on adaptive group lasso. *Computational statistics & data analysis*, 52(12):5277–5286.
- [Wang et al., 2018] Wang, Y.-C., Bohannon, R. W., Li, X., Sindhu, B., and Kapellusch, J. (2018). Hand-grip strength: normative reference values and equations for individuals 18 to 85 years of age residing in the united states. *Journal of Orthopaedic & Sports Physical Therapy*, 48(9):685–693.
- [Wang et al., 2021] Wang, Z., Sair, H. I., Crainiceanu, C., Lindquist, M., Landman, B. A., Resnick, S., et al. (2021). On statistical tests of functional connectome fingerprinting. *Canadian Journal of Statistics*, 49(1):63–88.
- [Wu and Politis, 2023] Wu, K. and Politis, D. N. (2023). Bootstrap prediction inference of non-linear autoregressive models. *arXiv preprint arXiv:2306.04126*.
- [Xu and Xie, 2021] Xu, C. and Xie, Y. (2021). Conformal prediction interval for dynamic time-series. In *International Conference on Machine Learning*, pages 11559–11569. PMLR.
- [Xu and Xie, 2023] Xu, C. and Xie, Y. (2023). Conformal prediction for time series. *IEEE Transactions on Pattern Analysis and Machine Intelligence*.
- [Yin et al., 2022] Yin, M., Shi, C., Wang, Y., and Blei, D. M. (2022). Conformal sensitivity analysis for individual treatment effects. *Journal of the American Statistical Association*, pages 1–14.
- [Zaffran et al., 2023] Zaffran, M., Dieuleveut, A., Josse, J., and Romano, Y. (2023). Conformal prediction with missing values. *arXiv preprint arXiv:2306.02732*.
- [Zhang et al., 2022] Zhang, Q., Li, B., and Xue, L. (2022). Nonlinear sufficient dimension reduction for distribution-on-distribution regression. *arXiv preprint arXiv:2207.04613*.
- [Zhang et al., 2018] Zhang, S., Cheng, D., Deng, Z., Zong, M., and Deng, X. (2018). A novel knn algorithm with data-driven k parameter computation. *Pattern Recognition Letters*, 109:44–54.
- [Zhang and Politis, 2022] Zhang, Y. and Politis, D. N. (2022). Bootstrap prediction intervals with asymptotic conditional validity and unconditional guarantees. *Information and Inference: A Journal of the IMA*, 12(1):157–209.
- [Zhong et al., 2023] Zhong, W., Li, Z., Guo, W., and Cui, H. (2023). Semi-distance correlation and its applications. *Journal of the American Statistical Association*, 0(ja):1–23.
- [Zhou and Müller, 2022] Zhou, Y. and Müller, H.-G. (2022). Network regression with graph laplacians. *Journal of Machine Learning Research*, 23(320):1–41.

## A Theory

### A.1 Homoscedastic case

#### A.1.1 Statistical consistency

**Proposition 7.** *Assume that Assumption 1 is satisfied. Then*

$$\frac{1}{n_2} \sum_{i \in [S_2]} |d_2(Y_i, m(X_i)) - d_2(Y_i, \tilde{m}(X_i))| = o_p(1). \quad (26)$$

Furthermore, for any continuity point  $v \in \mathbb{R}$  of  $G$  where  $G(v) = \mathbb{P}(d_2(Y, m(X)) \leq v)$ , we have:

$$|\tilde{G}^*(v) - G(v)| = o_p(1), \quad (27)$$

where  $\tilde{G}^*(v) = \frac{1}{n_2} \sum_{i \in [S_2]} \mathbb{I}\{d_2(Y_i, \tilde{m}(X_i)) \leq v\}$ .

*Proof.* For the first result, observe that

$$\frac{1}{n_2} \sum_{i \in [S_2]} |d_2(Y_i, m(X_i)) - d_2(Y_i, \tilde{m}(X_i))| \leq \frac{1}{n_2} \sum_{i \in [S_2]} |d_2(m(X_i), \tilde{m}(X_i))|.$$

By Assumption 1 and the law of large numbers, we have

$$\frac{1}{n_2} \sum_{i \in [S_2]} |d_2(Y_i, m(X_i)) - d_2(Y_i, \tilde{m}(X_i))| = o_p(1).$$

For the second part, fix  $v \in \mathbb{R}$  as a continuity point. Define  $\tilde{G}_m^*(v) = \frac{1}{n_2} \sum_{i \in [S_2]} \mathbb{I}\{d_2(Y_i, m(X_i)) \leq v\}$  and the random quantity  $R_T(v) = |\tilde{G}_m^*(v) - G(v)|$ , satisfying, by the law of large numbers,  $R_T(v) = o_p(1)$ . For any fixed  $\gamma > 0$ , define the set  $A_\gamma = \{i \in [S_2] : |d_2(Y_i, \tilde{m}(X_i)) - d_2(Y_i, m(X_i))| \geq \gamma\}$ . Then,

$$\begin{aligned} & n_2 \left[ \tilde{G}_m^*(v) - \tilde{G}^*(v) \right] \\ & \leq \left| \sum_{i \in A_\gamma} (\mathbb{I}\{d_2(Y_i, \tilde{m}(X_i)) \leq v\} - \mathbb{I}\{d_2(Y_i, m(X_i)) \leq v\}) \right| + \left| \sum_{i \in A_\gamma^c} (\mathbb{I}\{d_2(Y_i, \tilde{m}(X_i)) \leq v\}) - \mathbb{I}\{d_2(Y_i, m(X_i)) \leq v\} \right| \\ & \leq |A_\gamma| + \left| \sum_{i \in A_\gamma^c} (\mathbb{I}\{d_2(Y_i, \tilde{m}(X_i)) \leq v\} - \mathbb{I}\{d_2(Y_i, m(X_i)) \leq v\}) \right|. \end{aligned}$$

For  $i \in A_\gamma^c$ ,  $d_2(Y_i, m(X_i)) - \gamma \leq d_2(Y_i, \tilde{m}(X_i)) \leq d_2(Y_i, m(X_i)) + \gamma$ . Therefore,

$$\sum_{i \in A_\gamma^c} \mathbb{I}\{d_2(Y_i, m(X_i)) \leq v - \gamma\} \leq \sum_{i \in A_\gamma^c} \mathbb{I}\{d_2(Y_i, \tilde{m}(X_i)) \leq v\} \leq \sum_{i \in A_\gamma^c} \mathbb{I}\{d_2(Y_i, m(X_i)) \leq v + \gamma\}.$$

For any continuity point  $v \in \mathbb{R}^+$  and any  $\varepsilon_v > 0$ , there exists  $\delta_v > 0$  such that for any  $z \in (v - \delta_v, v + \delta_v)$ ,  $|G(z) - G(v)| < \varepsilon_v$ . Then,

$$n_2 \left| \tilde{G}^*(v) - \tilde{G}_m^*(v) \right|$$

$$\begin{aligned}
&\leq |A_\gamma| + \left| \sum_{i \in A_\gamma^c} \mathbb{I}\{d_2(Y_i, \tilde{m}(X_i)) \leq v\} - \sum_{i \in A_\gamma^c} \mathbb{I}\{d_2(Y_i, m(X_i)) \leq v\} \right| \\
&\leq |A_\gamma| + \left| n_2 \left[ \tilde{G}_m^*(v + \gamma) - \tilde{G}_m^*(v - \gamma) \right] - \left( \sum_{i \in A_\gamma} \mathbb{I}\{d_2(Y_i, m(X_i)) \leq v + \gamma\} - \sum_{i \in A_\delta} \mathbb{I}\{d_2(Y_i, m(X_i)) \leq v - \gamma\} \right) \right| \\
&\leq |A_\gamma| + n_2 \left( (G(v + \gamma)) - G(v - \gamma) + R_T(v + \gamma) + R_T(v - \gamma) \right) + |A_\gamma| \quad (\text{triangle inequality}) \\
&\leq n_2(2\varepsilon_v + R_T(v + \gamma) + R_T(v - \gamma)) + 2|A_\gamma|.
\end{aligned}$$

First letting  $n_2 \rightarrow \infty$  and then  $\gamma \rightarrow 0$ , we obtain

$$|\tilde{G}^*(v) - G(v)| \leq |\tilde{G}^*(v) - \tilde{G}_m^*(v)| + R_T(v) \leq o_p(1).$$

□

**Corollary 8.** *Assume that Assumption 1 is satisfied. For a fixed  $\alpha \in (0, 1)$ , let  $q_{1-\alpha} := \inf\{t \in \mathbb{R} : G(t) \geq 1 - \alpha\}$ , and suppose that  $q_{1-\alpha}$  exists uniquely and is a continuity point of  $G(\cdot)$ . For any  $\varepsilon > 0$ , as  $n_1 \rightarrow \infty$  and,  $n_2 \rightarrow \infty$ , we have*

$$\lim_{n_2 \rightarrow \infty} \mathbb{P}(|\tilde{q}_{1-\alpha}^m - q_{1-\alpha}| \geq \varepsilon) = 1,$$

and

$$\lim_{n_2 \rightarrow \infty} \mathbb{P}(|\tilde{q}_{1-\alpha} - q_{1-\alpha}| \geq \varepsilon) = 1,$$

where  $\tilde{q}_{1-\alpha}^m$  is the empirical quantile from the empirical distribution

$$\tilde{G}_m(t) = \frac{1}{n_2} \sum_{i \in [S_2]} \mathbb{I}\{d_2(Y_i, m(X_i)) \leq t\},$$

and  $\tilde{q}_{1-\alpha}$  is the empirical quantile from the empirical distribution

$$\tilde{G}^*(t) = \frac{1}{n_2} \sum_{i \in [S_2]} \mathbb{I}\{d_2(Y_i, \tilde{m}(X_i)) \leq t\}.$$

*Proof.* Both results are consequences of the law of large numbers, since  $\tilde{G}^*(q_{1-\alpha}) = G(q_{1-\alpha}) + o_p(1)$  and  $\tilde{G}_m^*(q_{1-\alpha}) = G(q_{1-\alpha}) + o_p(1)$ . □

## A.2 Proof of Theorem 3

The goal of this section is to show:

$$\int_{\mathcal{X}} \mathbb{P}(Y \in C^\alpha(x) \Delta \tilde{C}^\alpha(x) \mid X = x, \mathcal{D}_n) P_X(dx) = o_p(1),$$

where  $C^\alpha(x)$  and  $\tilde{C}^\alpha(x)$  are defined in Section 2.1.

*Proof.* For a fixed  $\alpha \in (0, 1)$ , let  $q_{1-\alpha}$  denote the corresponding quantile of  $d_2(Y, m(X))$ , and suppose that  $q_{1-\alpha}$  is a continuity point for the function  $G(\cdot)$ . Define the sets  $\tilde{C}_m^\alpha(x) = \mathcal{B}(m(x), \tilde{q}_{1-\alpha})$  and  $\tilde{C}_q^\alpha(x) = \mathcal{B}(\tilde{m}(x), q_{1-\alpha})$ , considering a fixed  $x \in \mathcal{X}$ . Define also the function  $G^*(t, x) = \mathbb{P}(d_2(Y, \tilde{m}(X)) \leq t \mid X = x)$ . Given the properties of the metric induced by the symmetric difference of two sets, it holds that

$$\begin{aligned}
& \mathbb{P}(Y \in C^\alpha(x) \Delta \tilde{C}^\alpha(x) \mid X = x, \mathcal{D}_n) \\
& \leq \mathbb{P}(Y \in C^\alpha(x) \Delta \tilde{C}_m^\alpha(x) \mid X = x, \mathcal{D}_n) + \mathbb{P}(Y \in \tilde{C}_m^\alpha(x) \Delta \tilde{C}^\alpha(x) \mid X = x, \mathcal{D}_n) \\
& \quad + \mathbb{P}(Y \in \tilde{C}^\alpha(x) \Delta \tilde{C}_q^\alpha(x) \mid X = x, \mathcal{D}_n) + \mathbb{P}(Y \in \tilde{C}_q^\alpha(x) \Delta \tilde{C}^\alpha(x) \mid X = x, \mathcal{D}_n).
\end{aligned}$$

We will analyze the four terms separately.

**Case 1:**

$$\begin{aligned}
& \mathbb{P}(Y \in C^\alpha(x) \Delta \tilde{C}_m^\alpha(x) \mid X = x, \mathcal{D}_n) \\
& = \mathbb{P}(\{Y : d_2(Y, m(X)) > q_{1-\alpha}, d_2(Y, m(X)) \leq \tilde{q}_{1-\alpha}\} \mid X = x, \mathcal{D}_n) \\
& \quad + \mathbb{P}(\{Y : d_2(Y, m(X)) \leq q_{1-\alpha}, d_2(Y, m(X)) > \tilde{q}_{1-\alpha}\} \mid X = x, \mathcal{D}_n) \\
& = 2|G(\tilde{q}_{1-\alpha}) - G(q_{1-\alpha})|.
\end{aligned}$$

Integrating, we have

$$\begin{aligned}
& \int_{\mathcal{X}} \mathbb{P}(Y \in C^\alpha(x) \Delta \tilde{C}_m^\alpha(x) \mid X = x, \mathcal{D}_n) P_X(dx) \\
& = 2|G(\tilde{q}_{1-\alpha}) - G(q_{1-\alpha})| \int_{\mathcal{X}} P_X(dx) = o_p(1),
\end{aligned}$$

and in combination with Corollary 8.

**Case 2:**

$$\begin{aligned}
& \mathbb{P}(Y \in \tilde{C}_m^\alpha(x) \Delta \tilde{C}^\alpha(x) \mid X = x, \mathcal{D}_n) \\
& = \mathbb{P}(\{Y : d(Y, m(X)) > \tilde{q}_{1-\alpha}, d_2(Y, \tilde{m}(X)) \leq \tilde{q}_{1-\alpha}\} \mid X = x, \mathcal{D}_n) \\
& \quad + \mathbb{P}(\{Y : d_2(Y, m(X)) \leq \tilde{q}_{1-\alpha}, d_2(Y, \tilde{m}(X)) > \tilde{q}_{1-\alpha}\} \mid X = x, \mathcal{D}_n) \\
& \leq \mathbb{P}(\{Y : d_2(Y, \tilde{m}(X)) \leq \tilde{q}_{1-\alpha} < d_2(\tilde{m}(X), m(X)) + d_2(y, \tilde{m}(X))\} \mid X = x, \mathcal{D}_n) \\
& \quad + \mathbb{P}(\{Y : d_2(Y, m(X)) \leq \tilde{q}_{1-\alpha} < d_2(\tilde{m}(X), m(X)) + d_2(Y, m(X))\} \mid X = x, \mathcal{D}_n) \\
& \leq G^*(\tilde{q}_{1-\alpha} + d_2(\tilde{m}(x), m(x)), x) - G^*(\tilde{q}_{1-\alpha}, x) + G(\tilde{q}_{1-\alpha} + d_2(\tilde{m}(x), m(x))) - G(\tilde{q}_{1-\alpha}).
\end{aligned}$$

Now, using the continuity hypothesis for  $q_{1-\alpha}$ ,  $\forall \varepsilon > 0$ , as  $n_1 \rightarrow \infty$ , and,  $n_2 \rightarrow \infty$ , we have

$$\lim_{n_2 \rightarrow \infty} \mathbb{P}(|\tilde{q}_{1-\alpha} - q_{1-\alpha}| \geq \varepsilon) = 1,$$

and that  $\mathbb{E}(d_2(\tilde{m}(X), m(X)) \mid \mathcal{D}_{\text{train}}) \rightarrow 0$  as  $|\mathcal{D}_{\text{train}}| \rightarrow \infty$ , we infer that  $\int_{\mathcal{X}} G^*(\tilde{q}_{1-\alpha} + d_2(\tilde{m}(x), m(x)), x) - G^*(\tilde{q}_{1-\alpha}, x) P_X(dx) = o_p(1)$ . Repeating for the other term, we have

$$\begin{aligned}
& \int_{\mathcal{X}} \mathbb{P}(Y \in \tilde{C}_m^\alpha(x) \Delta \tilde{C}^\alpha(x) \mid X = x, \mathcal{D}_n) P_X(dx) \\
& = \int_{\mathcal{X}} [G^*(\tilde{q}_{1-\alpha} + d_2(\tilde{m}(x), m(x)), x) - G^*(\tilde{q}_{1-\alpha}, x) + G(\tilde{q}_{1-\alpha} + d_2(\tilde{m}(x), m(x))) - G(\tilde{q}_{1-\alpha})] P_X(dx) = o_p(1).
\end{aligned}$$

**Case 3:**

$$\begin{aligned}
& \mathbb{P}(Y \in \tilde{C}^\alpha(x) \Delta \tilde{C}_q^\alpha(x) \mid X = x, \mathcal{D}_n) \\
&= \mathbb{P}(\{Y : d_2(Y, m(X)) > q_{1-\alpha}, d_2(Y, \tilde{m}(X)) \leq q_{1-\alpha}\} \mid X = x, \mathcal{D}_n) \\
&+ \mathbb{P}(\{Y : d_2(Y, m(X)) \leq q_{1-\alpha}, d_2(Y, \tilde{m}(X)) > q_{1-\alpha}\} \mid X = x, \mathcal{D}_n)
\end{aligned}$$

This is similar to Case 2, except that we exchange the role of  $\tilde{q}_{1-\alpha}$  with  $q_{1-\alpha}$ . Therefore, we have

$$\begin{aligned}
& \mathbb{P}(Y \in C^\alpha(x) \Delta \tilde{C}_q^\alpha(x) \mid X = x, \mathcal{D}_n) \\
&\leq G^*(q_{1-\alpha} + d_2(\tilde{m}(x), m(x), x) - G^*(q_{1-\alpha}, x) + G(q_{1-\alpha} + d_2(\tilde{m}(x), m(x)), x) - G(q_{1-\alpha}))
\end{aligned}$$

As a consequence,

$$\int_{\mathcal{X}} [G^*(q_{1-\alpha} + d_2(\tilde{m}(x), m(x), x) - G^*(q_{1-\alpha}, x) + G(q_{1-\alpha} + d_2(\tilde{m}(x), m(x)), x) - G(q_{1-\alpha}))] P_X(dx) = o_p(1).$$

#### Case 4:

Following the arguments of Case 1, we have that

$$\begin{aligned}
& \mathbb{P}(Y \in \tilde{C}_q^\alpha(x) \Delta \tilde{C}^\alpha(x) \mid X = x, \mathcal{D}_n) \\
&= \mathbb{P}(\{d_2(Y, \tilde{m}(x)) > q_{1-\alpha}, d_2(Y, \tilde{m}(x)) \leq \tilde{q}_{1-\alpha}\} \mid X = x, \mathcal{D}_n) \\
&+ \mathbb{P}(\{Y : d_2(Y, \tilde{m}(X)) \leq q_{1-\alpha}, d_2(Y, \tilde{m}(X)) > \tilde{q}_{1-\alpha}\} \mid X = x, \mathcal{D}_n),
\end{aligned}$$

and,

$$\mathbb{P}(Y \in \tilde{C}_q^\alpha(x) \Delta \tilde{C}^\alpha(x) \mid X = x, \mathcal{D}_n) \leq 2 |G^*(\tilde{q}_{1-\alpha}, x) - G^*(q_{1-\alpha}, x)| = o_p(1),$$

and as a consequence

$$\int_{\mathcal{X}} \mathbb{P}(Y \in \tilde{C}_q^\alpha(x) \Delta \tilde{C}^\alpha(x) \mid X = x, \mathcal{D}_n) P_X(dx) = o_p(1).$$

Finally, combining the prior four results, we infer that

$$\int_{\mathcal{X}} \mathbb{P}(Y \in C^\alpha(x) \Delta \tilde{C}^\alpha(x) \mid X = x, \mathcal{D}_n) P_X(dx) = o_p(1).$$

□

### A.3 Proof of Proposition 4

*Proof.* We begin by observing that, for the proof Proposition 4, we can decompose the probability of interest as follows:

$$\begin{aligned}
& \mathbb{P}(Y \in C^\alpha(x) \Delta \tilde{C}^\alpha(x) \mid X = x, \mathcal{D}_n) \\
&\leq \mathbb{P}(Y \in C^\alpha(x) \Delta \tilde{C}_m^\alpha(x) \mid X = x, \mathcal{D}_n) + \mathbb{P}(Y \in \tilde{C}_m^\alpha(x) \Delta \tilde{C}^\alpha(x) \mid X = x, \mathcal{D}_n) \\
&+ \mathbb{P}(Y \in \tilde{C}^\alpha(x) \Delta \tilde{C}_q^\alpha(x) \mid X = x, \mathcal{D}_n) + \mathbb{P}(Y \in \tilde{C}_q^\alpha(x) \Delta \tilde{C}^\alpha(x) \mid X = x, \mathcal{D}_n).
\end{aligned}$$

Now, for a fixed  $x \in \mathcal{X}$ , we decompose the four terms explicitly:

1.  $\mathbb{P}(Y \in C^\alpha(x) \Delta \tilde{C}_m^\alpha(x) \mid X = x, \mathcal{D}_n) = 2|G(\tilde{q}_{1-\alpha}^n) - G(q_{1-\alpha})|$
2.  $\mathbb{P}(Y \in \tilde{C}_m^\alpha(x) \Delta \tilde{C}^\alpha(x) \mid X = x, \mathcal{D}_n)$   
 $\leq G^*(\tilde{q}_{1-\alpha} + d_2(\tilde{m}(x), m(x)), x) - G^*(\tilde{q}_{1-\alpha}, x) + G(\tilde{q}_{1-\alpha} + d_2(\tilde{m}(x), m(x))) - G(\tilde{q}_{1-\alpha})$
3.  $\mathbb{P}(Y \in C^\alpha(x) \Delta \tilde{C}_q^\alpha(x) \mid X = x, \mathcal{D}_n)$   
 $\leq G^*(q_{1-\alpha} + d_2(\tilde{m}(x), m(x)), x) - G^*(q_{1-\alpha}, x) + G(q_{1-\alpha} + d_2(\tilde{m}(x), m(x))) - G(q_{1-\alpha})$
4.  $\mathbb{P}(Y \in \tilde{C}_q^\alpha(x) \Delta \tilde{C}^\alpha(x) \mid X = x, \mathcal{D}_n) = 2|G^*(\tilde{q}_{1-\alpha}, x) - G^*(q_{1-\alpha}, x)|$

First of all, we note that for the second and third terms, we use the fact that  $G$  and  $G^*$  are Lipschitz functions, and that we obtain an upper bound of the form  $Cd_2(\tilde{m}(x), m(x))$ .

For the first and fourth terms, we can provide an upper bound in terms of the distance between the population quantile and the empirical quantile. More specifically, we have

$$\mathbb{P}(Y \in C^\alpha(x) \Delta \tilde{C}_m^\alpha(x) \mid X = x, \mathcal{D}_n) + \mathbb{P}(Y \in \tilde{C}_q^\alpha(x) \Delta \tilde{C}^\alpha(x) \mid X = x, \mathcal{D}_n) \leq 4C|\tilde{q}_{1-\alpha} - q_{1-\alpha}|.$$

Now, integrating  $\int_{\mathcal{X}} \mathbb{P}(Y \in C^\alpha(x) \Delta \tilde{C}^\alpha(x) \mid X = x, \mathcal{D}_n) P_X(dx)$ , we obtain the desired results.  $\square$

#### A.4 Heteroscedastic case

To extend consisting results to the heteroscedastic scenario, we employ analogous arguments as in the homoscedastic case. The primary challenge arises from our use of a kNN algorithm to locally estimate the conditional distribution of distances,  $G(v, x) = \mathbb{P}(Y \in d_2(Y, m(X)) \leq v \mid X = x)$ , as applied in [Györfi and Walk, 2019]. For a given  $x \in \mathbb{R}^p$  and  $v \in \mathbb{R}$  as a continuity point, establishing convergence in probability crucially relies on the expression:

$$R_T(v, x) = |\tilde{G}_m^*(v, x) - G(v, x)| = o_p(1), \quad (28)$$

where  $\tilde{G}_m^*(v, x) = \frac{1}{k} \sum_{i \in N_k(x)} \mathbb{I}\{d_2(Y_i, m(X_i)) \leq v\}$ .

To address these challenges, we first establish some preliminary results.

**Theorem 9** (Strong consistency of kNN [Devroye, 1981]). *Let  $(X, Y), (X_1, Y_1), \dots, (X_n, Y_n)$  be independent identically distributed  $\mathbb{R}^p \times \mathbb{R}$ -valued random vectors with  $\mathbb{E}(|Y|) < \infty$ . The regression function  $m(x) = \mathbb{E}(Y \mid X = x)$ , for  $x \in \mathbb{R}^p$ , is estimated by*

$$\tilde{m}(x) = \frac{1}{k} \sum_{i \in N_k(x)} Y_i, \quad k \in \mathbb{N}. \quad (29)$$

Assume also that

$$|Y| \leq \gamma < \infty$$

and  $k = k_n$  is a sequence of integers such that  $\frac{k}{n} \rightarrow 0$  and  $k \rightarrow \infty$  as  $n \rightarrow \infty$ .

Then, for the nearest neighbor estimate,  $\mathbb{E}\{|\tilde{m}_n(x) - m(x)|\} \rightarrow 0$  as  $n \rightarrow \infty$  for almost all  $x \in \mathcal{X}$ , and  $\mathbb{E}\{|\tilde{m}_n(X) - m(X)|\} \rightarrow 0$  as  $n \rightarrow \infty$ . If, in addition,  $\frac{k}{\log n} \rightarrow \infty$  as  $k, n \rightarrow \infty$ , then

$$\mathbb{E}\{|\tilde{m}_n(X) - m(X)| \mid X_1, Y_1, \dots, X_n, Y_n\} \rightarrow 0 \text{ a.s.}$$

**Lemma 1.** Suppose that  $k \rightarrow \infty$  and  $\frac{k}{\log n} \rightarrow \infty$  as  $n \rightarrow \infty$  and hypothesis of Theorem 5 are satisfied. Then for almost every  $x \in \mathbb{R}^p$ ,

$$|\tilde{G}_m^*(v, x) - G(v, x)| = o_p(1) \text{ as } n \rightarrow \infty,$$

and

$$\mathbb{E}\{|\tilde{G}_m^*(v, x) - G(v, x)| | X_1, Y_1, \dots, X_n, Y_n\} = o_p(1) \text{ as } n \rightarrow \infty,$$

where  $\tilde{G}_m^*(v, x) = \frac{1}{k} \sum_{i \in N_k(x)} \mathbb{I}\{d_2(Y_i, m(X_i)) \leq v\}$ .

*Proof.* For a fixed positive  $v$  continuity point of  $G(v, x) = \mathbb{P}(d_2(Y, m(X)) \leq v | X = x)$ , define the function  $f : \mathbb{R}^p \times \mathbb{R} \rightarrow [0, 1]$  as  $f(x, y) = \mathbb{I}\{d_2(y, m(x)) \leq v\}$ . Consider

$$\tilde{m}(x) = \frac{1}{k} \sum_{i=1}^k f(X_{(i)}(x), Y_{(i)}(x)) = \tilde{G}_m^*(v, x).$$

Note that

$$|\tilde{G}_m^*(v, x) - G(v, x)| = \left| \frac{1}{k} \sum_{i=1}^k f(X_{(i)}(x), Y_{(i)}(x)) - \mathbb{E}[f(X, Y) | X = x] \right|. \quad (30)$$

Now, define the random variable  $Y' = f(X, Y)$ , and the pair  $(X, Y') \in \mathbb{R}^p \times \mathbb{R}$  satisfies the conditions of Theorem 9, where we obtain:

$$|\tilde{G}_m^*(v, x) - G(v, x)| = o_p(1) \text{ as } n \rightarrow \infty, \quad (31)$$

and

$$\mathbb{E}\{|\tilde{G}_m^*(v, x) - G(v, x)| | X_1, Y_1, \dots, X_n, Y_n\} \rightarrow 0 \text{ a.s as } n \rightarrow \infty. \quad \square$$

#### A.4.1 Statistical consistency

**Proposition 10.** Assume that Assumption 3 holds. For every fixed  $x \in \mathcal{X}$ , and  $v \in \mathbb{R}$  is a continuity point of  $G(v, x) = \mathbb{P}(d_2(Y, m(X)) \leq v | X = x)$ , and  $k \in \mathbb{N}$  satisfying the regularity conditions from Theorem 5, then

$$|\tilde{G}^*(v, x) - G(v, x)| = o_p(1), \quad (32)$$

where  $\tilde{G}^*(v, x) = \frac{1}{k} \sum_{i \in N_k(x)} \mathbb{I}\{d_2(Y_i, \tilde{m}(X_i)) \leq v\}$ .

*Proof.* Fix  $v \in \mathbb{R}$  as a continuity point. Define  $\tilde{G}_m^*(v, x) = \frac{1}{k} \sum_{i \in N_k(x)} \mathbb{I}\{d_2(Y_i, m(X_i)) \leq v\}$  and  $R_T(v, x) = |\tilde{G}_m^*(v, x) - G(v, x)|$ . By Lemma 1  $R_T(v, x) = o_p(1)$ , for almost every  $x \in \mathbb{R}^p$ .

For any fixed  $\gamma > 0$ , define the set  $A_\gamma = \{i \in N_k(x) : |d_2(Y_i, \tilde{m}(X_i)) - d_2(Y_i, m(X_i))| \geq \gamma\}$ . Then,

$$\begin{aligned} & k \left[ \tilde{G}_m^*(v, x) - \tilde{G}^*(v, x) \right] \\ & \leq \left| \sum_{i \in A_\gamma} (\mathbb{I}\{d_2(Y_i, \tilde{m}(X_i)) \leq v\} - \mathbb{I}\{d_2(Y_i, m(X_i)) \leq v\}) \right| + \left| \sum_{i \in A_\gamma^c} (\mathbb{I}\{d_2(Y_i, \tilde{m}(X_i)) \leq v\}) - \mathbb{I}\{d_2(Y_i, m(X_i)) \leq v\} \right| \\ & \leq |A_\gamma| + \left| \sum_{i \in A_\gamma^c} (\mathbb{I}\{d_2(Y_i, \tilde{m}(X_i)) \leq v\} - \mathbb{I}\{d_2(Y_i, m(X_i)) \leq v\}) \right|. \end{aligned}$$

For  $i \in A_\gamma^c$ ,  $d_2(Y_i, m(X_i)) - \gamma \leq d_2(Y_i, \tilde{m}(X_i)) \leq d_2(Y_i, m(X_i)) + \gamma$ . Therefore,

$$\sum_{i \in A_\gamma^c} \mathbb{I}\{d_2(Y_i, m(X_i)) \leq v - \gamma\} \leq \sum_{i \in A_\gamma^c} \mathbb{I}\{d_2(Y_i, \tilde{m}(X_i)) \leq v\} \leq \sum_{i \in A_\gamma^c} \mathbb{I}\{d_2(Y_i, m(X_i)) \leq v + \gamma\}.$$

For a fixed  $x \in \mathbb{R}^p$ , and any continuity point  $v \in \mathbb{R}^+$  and any  $\varepsilon_v > 0$ , there exists  $\delta_v > 0$  such that for any  $z \in (v - \delta_v, v + \delta_v)$ ,  $|G(z, x) - G(v, x)| < \varepsilon_v$ . Then,

$$\begin{aligned}
& k \left| \tilde{G}^*(v, x) - \tilde{G}_m(v, x) \right| \\
& \leq |A_\gamma| + \left| \sum_{i \in A_\gamma^c} \mathbb{I}\{d_2(Y_i, \tilde{m}(X_i)) \leq v\} - \sum_{i \in A_\gamma^c} \mathbb{I}\{d_2(Y_i, m(X_i)) \leq v\} \right| \\
& \leq |A_\gamma| + \left| k \left[ \tilde{G}_m^*(v + \gamma, x) - \tilde{G}_m(v - \gamma, x) \right] - \left( \sum_{i \in A_\gamma} \mathbb{I}\{d_2(Y_i, m(X_i)) \leq v + \gamma\} - \sum_{i \in A_\delta} \mathbb{I}\{d_2(Y_i, m(X_i)) \leq v - \gamma\} \right) \right| \\
& \leq |A_\gamma| + k \left( (G(v + \gamma, x) - G(v - \gamma, x) + R_T(v + \gamma, x) + R_T(v - \gamma, x)) + |A_\gamma| \right) \quad (\text{triangle inequality}) \\
& \leq k(2\varepsilon_v + R_T(v + \gamma, x) + R_T(v - \gamma, x)) + 2|A_\gamma|.
\end{aligned}$$

First letting  $n_2 \rightarrow \infty$ ,  $k \rightarrow \infty$  and  $\gamma \rightarrow 0$ , we obtain

$$|\tilde{G}^*(v, x) - G(v, x)| \leq |\tilde{G}^*(v, x) - \tilde{G}_m(v, x)| + R_T(v, x) \leq o_p(1).$$

□

**Corollary 11.** Assume that Assumption 3 is satisfied. For a fixed  $x \in \mathcal{X}$ , and  $\alpha \in (0, 1)$ , let  $q_{1-\alpha}(x) := \inf\{t \in \mathbb{R} : G(t, x) \geq 1 - \alpha\}$ , and suppose that  $q_{1-\alpha}(x)$  exists uniquely and is a continuity point of  $G(\cdot, x)$ .  $\forall \varepsilon > 0$ , as  $n_1 \rightarrow \infty$ ,  $n_2 \rightarrow \infty$ ,  $k \rightarrow \infty$  we have

$$\lim_{k \rightarrow \infty} \lim_{n_2 \rightarrow \infty} \mathbb{P}(|\tilde{q}_{1-\alpha}^m(x) - q_{1-\alpha}(x)| \geq \varepsilon) = 1,$$

and

$$\lim_{k \rightarrow \infty} \lim_{n_2 \rightarrow \infty} \mathbb{P}(|\tilde{q}_{1-\alpha}(x) - q_{1-\alpha}(x)| \geq \varepsilon) = 1.$$

## A.5 Proof of Theorem 5

The goal of this proof is to show:

$$\int_{\mathcal{X}} \mathbb{P}(Y \in C^\alpha(x) \Delta \tilde{C}^\alpha(x) \mid X = x, \mathcal{D}_n) P_X(dx) = o_p(1),$$

where  $C^\alpha(x)$  and  $\tilde{C}^\alpha(x)$  are defined as before.

*Proof.* For a fixed  $x \in \mathbb{R}^p$ , and  $\alpha \in (0, 1)$ , let  $q_{1-\alpha}(x)$  denote the corresponding quantile of  $d_2(Y, m(X)) \mid X = x$ , and suppose that  $q_{1-\alpha}(x)$  is a continuity point for the function  $G(\cdot, x)$ . Define the sets  $\tilde{C}_m^\alpha(x) = \mathcal{B}(m(x), \tilde{q}_{1-\alpha}(x))$  and  $\tilde{C}_q^\alpha(x) = \mathcal{B}(\tilde{m}(x), q_{1-\alpha}(x))$ , considering a fixed  $x \in \mathcal{X}$ . Define also the function  $G^*(t, x) = \mathbb{P}(d_2(Y, \tilde{m}(X)) \leq t \mid X = x)$ . Given the properties of the metric induced by the symmetric difference of two sets, it holds that

$$\begin{aligned}
& \mathbb{P}(Y \in C^\alpha(x) \Delta \tilde{C}^\alpha(x) \mid X = x, \mathcal{D}_n) \\
& \leq \mathbb{P}(Y \in C^\alpha(x) \Delta \tilde{C}_m^\alpha(x) \mid X = x, \mathcal{D}_n) + \mathbb{P}(Y \in \tilde{C}_m^\alpha(x) \Delta \tilde{C}^\alpha(x) \mid X = x, \mathcal{D}_n)
\end{aligned}$$

$$+ \mathbb{P}(Y \in C^\alpha(x) \Delta \tilde{C}_q^\alpha(x) \mid X = x, \mathcal{D}_n) + \mathbb{P}(Y \in \tilde{C}_q^\alpha(x) \Delta \tilde{C}^\alpha(x) \mid X = x, \mathcal{D}_n).$$

We will analyze the four terms separately.

**Case 1:**

$$\begin{aligned} & \mathbb{P}(Y \in C^\alpha(x) \Delta \tilde{C}_m^\alpha(x) \mid X = x, \mathcal{D}_n) \\ &= \mathbb{P}(\{Y : d_2(Y, m(X)) > q_{1-\alpha}(x), d_2(Y, m(X)) \leq \tilde{q}_{1-\alpha}(x)\} \mid X = x, \mathcal{D}_n) \\ & \quad + \mathbb{P}(\{Y : d_2(Y, m(X)) \leq q_{1-\alpha}(x), d_2(Y, m(X)) > \tilde{q}_{1-\alpha}(x)\} \mid X = x, \mathcal{D}_n) \\ &= 2|G(\tilde{q}_{1-\alpha}(x), x) - G(q_{1-\alpha}(x), x)|. \end{aligned}$$

Integrating, we have

$$\begin{aligned} & \int_{\mathcal{X}} \mathbb{P}(Y \in C^\alpha(x) \Delta \tilde{C}_m^\alpha(x) \mid X = x, \mathcal{D}_n) P_X(dx) \\ &= 2|G(\tilde{q}_{1-\alpha}(x), x) - G(q_{1-\alpha}(x), x)| \int_{\mathcal{X}} P_X(dx) = o_p(1), \end{aligned}$$

and in combination with Corollary 11.

**Case 2:**

$$\begin{aligned} & \mathbb{P}(Y \in \tilde{C}_m^\alpha(x) \Delta \tilde{C}^\alpha(x) \mid X = x, \mathcal{D}_n) \\ &= \mathbb{P}(\{Y : d(Y, m(X)) > \tilde{q}_{1-\alpha}(x), d_2(Y, \tilde{m}(X)) \leq \tilde{q}_{1-\alpha}(x)\} \mid X = x, \mathcal{D}_n) + \\ & \mathbb{P}(\{Y : d_2(Y, m(X)) \leq \tilde{q}_{1-\alpha}(x), d_2(Y, \tilde{m}(X)) > \tilde{q}_{1-\alpha}(x)\} \mid X = x, \mathcal{D}_n) \\ &\leq \mathbb{P}(\{Y : d_2(Y, \tilde{m}(X)) \leq \tilde{q}_{1-\alpha}(x) < d_2(\tilde{m}(X), m(X)) + d_2(y, \tilde{m}(X))\} \mid X = x, \mathcal{D}_n) + \\ & \mathbb{P}(\{Y : d_2(Y, m(X)) \leq \tilde{q}_{1-\alpha}(x) < d_2(\tilde{m}(X), m(X)) + d_2(Y, m(X))\} \mid X = x, \mathcal{D}_n) \\ &\leq G^*(\tilde{q}_{1-\alpha}(x) + d_2(\tilde{m}(x), m(x)), x) - G^*(\tilde{q}_{1-\alpha}(x), x) + G(\tilde{q}_{1-\alpha}(x) + d_2(\tilde{m}(x), m(x)), x) - G(\tilde{q}_{1-\alpha}(x), x). \end{aligned}$$

Now, using the continuity hypothesis for  $q_{1-\alpha}(x)$ ,  $\forall \varepsilon > 0$ , as  $n_1 \rightarrow \infty$ ,  $n_2 \rightarrow \infty$ , and  $k \rightarrow \infty$  we have

$$\lim_{k \rightarrow \infty} \lim_{n_2 \rightarrow \infty} \mathbb{P}(|\tilde{q}_{1-\alpha}^m(x) - q_{1-\alpha}(x)| \geq \varepsilon) = 1,$$

and

$$\lim_{n_2 \rightarrow \infty} \mathbb{P}(|\tilde{q}_{1-\alpha}(x) - q_{1-\alpha}(x)| \geq \varepsilon) = 1,$$

and that  $\mathbb{E}(d_2(\tilde{m}(X), m(X)) \mid \mathcal{D}_{\text{train}}) \rightarrow 0$  as  $|\mathcal{D}_{\text{train}}| \rightarrow \infty$ , we infer that  $\int_{\mathcal{X}} G^*(\tilde{q}_{1-\alpha}(x) + d_2(\tilde{m}(x), m(x)), x) - G^*(\tilde{q}_{1-\alpha}(x), x) P_X(dx) = o_p(1)$ . Repeat for the other term, we have

$$\begin{aligned} & \int_{\mathcal{X}} \mathbb{P}(Y \in \tilde{C}_m^\alpha(x) \Delta \tilde{C}^\alpha(x) \mid X = x, \mathcal{D}_n) P_X(dx) \\ &= \int_{\mathcal{X}} [G^*(\tilde{q}_{1-\alpha}(x) + d_2(\tilde{m}(x), m(x)), x) - G^*(\tilde{q}_{1-\alpha}(x), x) \\ & \quad + G(\tilde{q}_{1-\alpha}(x) + d_2(\tilde{m}(x), m(x)), x) - G(\tilde{q}_{1-\alpha}(x), x)] P_X(dx) = o_p(1). \end{aligned}$$

**Case 3:**

$$\begin{aligned}
& \mathbb{P}(Y \in C^\alpha(x) \Delta \tilde{C}_q^\alpha(x) \mid X = x, \mathcal{D}_n) \\
&= \mathbb{P}(\{Y : d_2(Y, m(X)) > q_{1-\alpha}(x), d_2(Y, \tilde{m}(X)) \leq q_{1-\alpha}(x)\} \mid X = x, \mathcal{D}_n) \\
&+ \mathbb{P}(\{Y : d_2(Y, m(X)) \leq q_{1-\alpha}(x), d_2(Y, \tilde{m}(X)) > q_{1-\alpha}(x)\} \mid X = x, \mathcal{D}_n).
\end{aligned}$$

This is similar to Case 2, except that we exchange the role of  $\tilde{q}_{1-\alpha}(x)$  with  $q_{1-\alpha}(x)$ . Therefore, we have

$$\begin{aligned}
& \mathbb{P}(Y \in C^\alpha(x) \Delta \tilde{C}_q^\alpha(x) \mid X = x, \mathcal{D}_n) \\
&\leq G^*(q_{1-\alpha}(x) + d_2(\tilde{m}(x), m(x), x) - G^*(q_{1-\alpha}(x), x) + G(q_{1-\alpha}(x) + d_2(\tilde{m}(x), m(x), x) - G(q_{1-\alpha}(x), x), x).
\end{aligned}$$

As a consequence,

$$\int_{\mathcal{X}} [G^*(q_{1-\alpha}(x) + d_2(\tilde{m}(x), m(x), x) - G^*(q_{1-\alpha}(x), x) + G(q_{1-\alpha}(x) + d_2(\tilde{m}(x), m(x), x) - G(q_{1-\alpha}(x), x), x)] P_X(dx) = o_p(1).$$

**Case 4:**

Following the arguments of Case 1, we have that

$$\begin{aligned}
& \mathbb{P}(Y \in \tilde{C}_q^\alpha(x) \Delta \tilde{C}^\alpha(x) \mid X = x, \mathcal{D}_n) \\
&= \mathbb{P}(\{d_2(Y, \tilde{m}(X)) > q_{1-\alpha}(x), d_2(Y, \tilde{m}(X)) \leq \tilde{q}_{1-\alpha}(x)\} \mid X = x, \mathcal{D}_n) \\
&+ \mathbb{P}(\{Y : d_2(Y, \tilde{m}(X)) \leq q_{1-\alpha}(x), d_2(Y, \tilde{m}(X)) > \tilde{q}_{1-\alpha}(x)\} \mid X = x, \mathcal{D}_n),
\end{aligned}$$

and,

$$\mathbb{P}(Y \in \tilde{C}_q^\alpha(x) \Delta \tilde{C}^\alpha(x) \mid X = x, \mathcal{D}_n) \leq 2 | G^*(\tilde{q}_{1-\alpha}(x), x) - G^*(q_{1-\alpha}(x), x)| = o_p(1),$$

and as a consequence

$$\int_{\mathcal{X}} \mathbb{P}(Y \in \tilde{C}_q^\alpha(x) \Delta \tilde{C}^\alpha(x) \mid X = x, \mathcal{D}_n) P_X(dx) = o_p(1).$$

Finally, combining the prior four results, we infer that

$$\int_{\mathcal{X}} \mathbb{P}(Y \in C^\alpha(x) \Delta \tilde{C}^\alpha(x) \mid X = x, \mathcal{D}_n) P_X(dx) = o_p(1).$$

□